Utrecht University

MCC Materials Chemistry and Catalysis

Master's Thesis

The Influence of Pd-Ni/SBA-15 Nanoparticle Composition on Selective Hydrogenation Catalysis

Kyra M. van Nieuwkerk, Bsc.

4 April 2023

Daily Supervisor:
Kristiaan H. Helfferich, Msc.

First Examiner:
Prof. Dr. Petra E. de Jongh

Second Examiner:
Dr. Jessi E. S. van der Hoeven

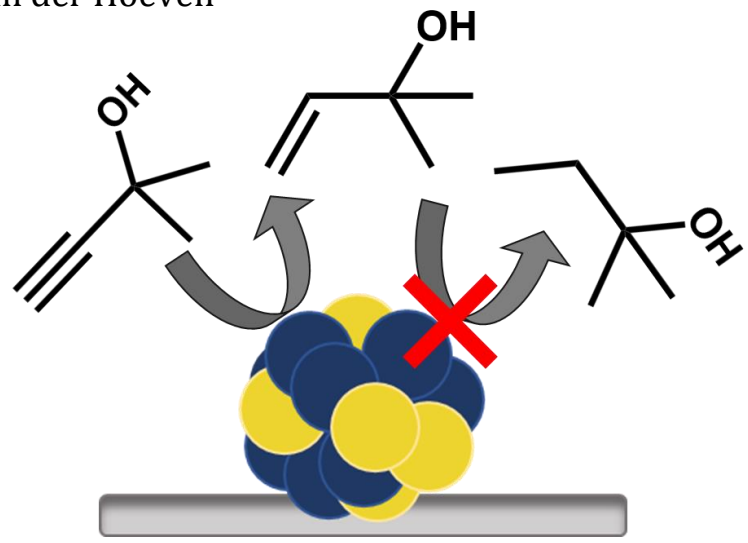

Materials Chemistry and Catalysis
Department of Chemistry
Debye Institute for Nanomaterials Science

Lay Summary

Hydrogenation reactions – reactions with hydrogen – are used in the production of many everyday goods, including perfumes, plastics, and pharmaceutics. These processes typically require a catalyst. Catalysts are particles that accelerate the rate of a reaction and improve the yield of the desired product without being consumed. In hydrogenation reactions, metal nanoscale (0.000000001 m) particles comprising of palladium (Pd) or nickel (Ni) usually function as the catalyst. However, recent studies have shown that combining these two metals in one particle can modify and even enhance their catalytic properties. These properties can be tuned and potentially optimized by varying the relative amounts of Pd and Ni (the composition) within the particles. Therefore, this thesis focused on the preparation and catalysis of nanoscale catalysts with different amounts of Pd compared to Ni. First, we made the catalysts with a facile and industrially relevant preparation technique. Then, we investigated the effects of composition on the rate and the yield of the desired product in three different liquid phase hydrogenation reactions. Their stability (if their structure remained unaltered during catalysis) was also studied. We found that these properties depended on both the composition of the catalyst and the reaction. In two reactions, an increasing amount of Pd relative to Ni slowed the reaction down. The opposite was true for the other reaction; the rate increased with the amount of Pd in the particles. In general, Pd decreased the yield to the desired product in two reactions. This was not evident in another. The stability of the catalyst also depended on the composition in two of the reactions, but not in the third one. Our findings show the importance of selecting the right composition and reaction for optimal catalytic performance.

Abstract

Approximately 25% of chemical processes involve at least one hydrogenation step. Most rely on heterogeneous catalysts. A promising way to improve the efficiency of these processes is to combine two metals, such as Pd and Ni, in one nanoparticle (NP). Catalytic performance can be tuned by varying the composition. In this thesis, alloyed Pd-Ni/SBA-15 NPs of different atomic ratios (Pd:Ni 1:20, 1:15, 1:10, and 1:7) were prepared by incipient wetness co-impregnation. Structure-performance relationships were investigated in the liquid phase selective hydrogenation of: cinnamaldehyde (CAL), citral, and 2-methyl-3-butyn-2-ol (MBY). The activity, selectivity, and stability of the Pd-Ni/SBA-15 catalysts were compared to that of Pd/SBA-15 and Ni/SBA-15. Characterization with HAADF STEM(-EDX), H_2-TPR, and powder XRD showed that we could change the composition of the Pd-Ni/SBA-15 NPs to the target ratio, without significantly affecting the particle size or nanoscale intimacy of the two metals. The NPs were homogeneously distributed over the support. The performance of the model catalysts relied on the composition and model reaction. In the hydrogenation of CAL, the activity of the Pd-Ni/SBA-15 NPs additively increased with the Pd content. All bimetallic catalysts were slightly less selective (1-3 %) to the main product (hydrocinnamaldehyde) compared to Ni/SBA-15. Compared to Pd/SBA-15, they showed a greater resistance to leaching. In the reduction of citral, the same general trend in the selectivity to the main product (citronellal) and stability was found. However, in this reaction, an increasing Pd content in the Pd-Ni/SBA-15 NPs reduced the activity. In the semi-hydrogenation of MBY, a similar composition-activity relationship was observed. All bimetallic catalysts had a higher selectivity to 2-methyl-3-buten-2-ol than Pd/SBA-15. No evidence of leaching was found. Our findings demonstrate the importance of selecting the right composition and (model) reaction for optimal catalytic performance.

Contents

List of Abbreviations

CAL	Cinnamaldehyde
COL	Cinnamic alcohol
EDX	Energy-Dispersive X-ray spectroscopy
GC	Gas Chromatograph
HAADF STEM	High-Angle Annular Dark-Field Scanning Transmission Electron Microscopy
HCAL	Hydrocinnamaldehyde
HCOL	Hydrocinnamic alcohol
ICP-OES	Inductively Coupled Plasma - Optical Emission Spectroscopy
MBA	2-Methyl-3-butan-2-ol
MBE	2-Methyl-3-buten-2-ol
MBY	2-Methyl-3-butyn-2-ol
NP	Nanoparticle
TOF	Turnover Frequency
TPR	Temperature-Programmed Reduction
XCAD	External Catalyst Addition Device
XRD	X-Ray Diffraction

1

Introduction

1.1 Hydrogenation catalysis

Approximately 25% of industrial processes involve at least one hydrogenation step.[1] From the manufacturing of fertilizers, pharmaceutics, and fragrances to the production of fuels: hydrogenation reactions are at the heart of the chemical industries.[2–5] Most hydrogenation processes rely on a heterogeneous catalyst.[6,7] In this case, a solid is used to increase the rate of a liquid or gas phase reaction. Metal nanoparticles (NPs) (<100 nm) often serve as the catalyst due to their increased surface area and unique chemical properties.[8] To prevent sintering, these particles are embedded in a high-surface-area-support (i.e. a porous support).

To maximize the efficiency of hydrogenation processes, these NPs must not only be very stable and active, but also highly selective.[9,10] The synthesis of important industrial intermediates typically involves the hydrogenation of unsaturated functional groups such as C=C, C≡C, and C=O to their corresponding alkanes, alkenes, and alcohols. Reactants often possess multiple functional groups, while only one needs to be reduced. Alternatively, the semi-hydrogenation of one functional group (e.g. C≡C → C=C) is required and over-hydrogenation (to C−C) must be prevented.

1.2 Bimetallic catalysis

Noble metals such as palladium and platinum, or base metals like nickel, are among the most widely used metals in hydrogenation catalysis.[7] However, recent studies have shown that bringing two different metals together at the nanoscale can modify and even enhance catalytic performance.[11] In some hydrogenation reactions, synergistic effects have been reported.[12,13] Herein, the catalytic properties of the bimetallic NPs exceed those of their monometallic counterparts.

The distinct catalytic properties of bimetallic NPs are generally the result of electronic and/or geometric effects.[14]

1) Electronic effects
   In this case, the interactions between two metal species change the electronic properties of the active sites.[15] This is typically understood in terms of the shift in d-band center

triggered by electron transfer from the more electropositive metal to the electronegative metal. Consequently, the adsorption strength of reactants/products is altered.[16] This can affect catalytic activity and selectivity.[17]

2) Geometric effects
   Bimetallic NPs are also geometrically different from their parent metals.[15,18–21] This includes changes in interatomic bond lengths and in the ensemble size of the active sites. The isolation of Pd atoms through alloying has, for instance, been shown to improve selectivity in hydrogenation reactions by changing the preferred adsorption mode of the reactant.[22]

For bimetallic NPs, composition is a key factor in catalytic performance.[19,23] By altering the ratio of the two metals within the NPs, the electronic and geometric properties of the active sites can be modified even more.[24] This flexibility in structure offers a unique opportunity to further optimize catalytic performance. Hence, it is crucial to control NP composition and understand its effect on hydrogenation catalysis.

1.3 Palladium and nickel

The choice of metals is often motivated by their individual (catalytic) properties. This work focusses on Pd-Ni NPs. Palladium tends to be very active in hydrogenation reactions, even under mild conditions.[25] However, its low abundancy and high price is an incentive to minimize its use. Nickel, although typically less active, is considerable more abundant and economical.[26] It also possesses a high alloying efficiency with noble metals. This makes it easier to achieve the nanoscale intimacy between Pd and Ni necessary to tune catalytic performance. Combining minimal amounts of Pd with Ni may therefore be a way to cut costs, as well as improve catalytic performance.[27,28]

1.4 Synthesis

Uncovering the effects of Pd-Ni NP composition on catalytic performance requires catalysts with a precise size, shape, and composition. However, well-defined bimetallic particles are complicated to prepare.[29] Each metal has different thermodynamic and kinetic properties under the same reaction conditions. Phase separation, undesired structures (e.g. core-shell instead of alloyed), and/or inhomogeneous compositions are therefore common problems in the synthesis of bimetallic catalysts.[30] These problems may be circumvented through careful selection of the preparation technique.[31]

Deposition precipitation and colloidal routes are among the most controllable methods, while impregnation tends to produce inhomogeneous particle sizes, compositions, and distributions.[31–34] Nevertheless, impregnation is the preferred method in industry due to its easy execution, low waste streams, and scalability.[34] In this work, we show that we can use this technique to prepare well-defined Pd-Ni catalysts with different compositions. This is achieved by making use of the strongly dispersing power of ethylenediamine – a bidentate chelating agent.

1.5 Aims and approach

Although some accounts on the effects of Pd-Ni NP composition on hydrogenation catalysis exist, much is still unknown.[27,28,35–37] Studies on Pd-Ni NPs with a predominantly Ni character are, for example, scarce.[28] Moreover, many works only focus on activity and selectivity, but neglect catalytic stability.[28,36] In other cases, it is unclear if the compositional changes did not affect the particle size and/or nanoscale intimacy between the two metals.[35] The influence of composition on catalytic performance may therefore have been convoluted with other effects. Hence, this thesis aimed to:

1) Prepare uniformly sized alloyed Pd-Ni/SBA-15 catalysts of different compositions with dilute amounts of Pd.
2) Examine Pd-Ni/SBA-15 NP structure-performance relationships in selective hydrogenation reactions and compare the activity, selectivity, and stability to Pd/SBA-15 and Ni/SBA-15

To this end, incipient wetness (co-)impregnation was used to synthesize alloyed Pd-Ni NPs of different Pd:Ni (atomic) ratios: 1:20, 1:15, 1:10, and 1:7, as well as monometallic reference catalysts. The NPs were characterized by Scanning Transmission Electron Microscopy with Energy Dispersive X-ray spectroscopy (STEM-EDX), powder X-Ray Diffraction (XRD), and Hydrogen Temperature-Programmed Reduction (H_2-TPR). Structure-performance relationships were investigated for the selective hydrogenation of three liquid phase reactions: 1) cinnamaldehyde, 2) citral, and 3) 2-methyl-3-butyn-2-ol.

2

Theory

2.1 Impregnation

In general, catalyst synthesis by impregnation consists of 3 steps: 1) Impregnation, 2) drying, and 3) activation.[34] A schematic overview of this process in given in Figure 1.

1) Impregnation

First, the precursor solution must be contacted with a porous support.[34] Typical precursors are inorganic metal salts such as nitrates and acetates in an aqueous solution. Chelating agents, e.g. ethylenediamine, are sometimes added, as the formation of chelated metal complexes can lead to better defined catalysts and a more uniform distribution of NPs over the support.[38] The support is impregnated with an amount of precursor equal to the pore volume (incipient wetness impregnation) or in excess of the pore volume (wet impregnation).[31] The former is often preferred, as it prevents the (uncontrolled) deposition of metals on the external support surface. In bimetallic NP synthesis, there are two variations on the aforementioned impregnation techniques: separate precursor solutions can be prepared for each metal with which the support is sequentially impregnated.[39] Alternatively, both metals are dissolved in one precursor solution and the pores are impregnated in one step (co-impregnation). Co-impregnation is more commonly employed for alloyed NPs.[39]

2) Drying

After capillary forces have forced the precursor into the pores, the support is dried.[34] During this process, the concentration of the precursor increases and the metal salts precipitate. The

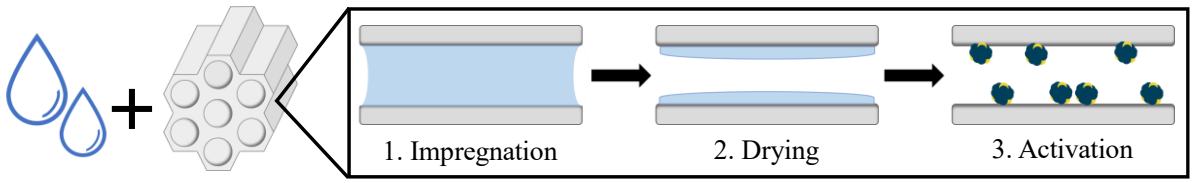

Figure 1. Schematic overview of the general steps in the preparation of supported nanocatalysts by impregnation.

drying step only greatly influences the distribution of metals if they weakly adsorb to the support.

3) Activation

In this step, NPs form and the active catalyst is obtained.[34] In general, a calcination step (heat treatment in air) is followed by a reduction step. The former typically results in metal oxides. These become metallic during the reduction step, often performed in H_2 (g) under elevated temperatures. The temperature (ramp) and gas flow are important parameters, as they can greatly influence the metal distribution.[40,41]

2.2 Selective hydrogenation

2.2.1 α,β-Unsaturated aldehydes

One important class of selective hydrogenation reactions are α,β-unsaturated aldehydes.[4] This transformation is employed in the synthesis of fine chemicals in the fragrance, flavor, and pharmaceutical industry. In the reduction of α,β-unsaturated aldehydes, both the C=O and the C=C bond can be hydrogenated, as presented in Figure 2. The hydrogenation of the former yields the unsaturated alcohol, while the reduction of the latter generates the saturated aldehyde. Which one is preferred depends on the application.[42] The low value saturated alcohol is produced when both groups are hydrogenated.

The saturated aldehyde is typically formed the most, owing to the lower bond- and adsorption energy of the C=C group.[43] Studies therefore tend to focus on increasing the selectivity to the C=O bond.[44] Nevertheless, developing high performing catalysts with an excellent C=C bond selectivity is still a great challenge.[4] In general, selectivity is correlated with the metal d-band width. Catalysts with a more narrow d-band favor C=C hydrogenation.[43] Palladium and Ni both have a relatively narrow d-band.[45] However, the more broad d-band of Pd compared to Ni make this metal less selective to the saturated aldehyde.[42] Enhanced catalytic properties have been reported for bimetallic Pd-Ni NPs, though these still do not always meet industrial selectivity demands.[4,28,35]

The unique reaction pathways, in combination with the difficulty of obtaining a high selectivity to either the unsaturated alcohol or the saturated aldehyde, make the hydrogenation of α,β-unsaturated aldehydes a good model reaction for fundamental studies on structure-performance relationships.[4] The selective hydrogenation of cinnamaldehyde and citral – two α,β-unsaturated aldehydes – are therefore interesting candidates for uncovering Pd-Ni/SBA-15 structure-performance relationship.

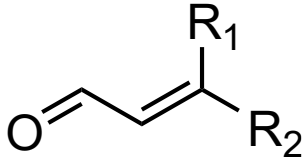

Figure 2. General structure of an α,β-unsaturated aldehyde with its characteristic C=O and C=C group. Both can be hydrogenated.

Cinnamaldehyde

Cinnamaldehyde (CAL) is a simple and easy-to-handle α,β-unsaturated aldehyde.[46] Figure 3 shows the reaction scheme. The main hydrogenation products are hydrocinnamaldehyde (HCAL) and cinnamic alcohol (COL). The over-hydrogenation of either one generates hydrocinnamic alcohol (HCOL). Palladium and nickel are both highly selective to HCAL, with maximum selectivities of over 90% reported in literature.[46,47] Palladium is more active, due to its lower activation energy for hydrogen adsorption and dissociation.[46] The hydrogenation of CAL is sensitive to Pd-Ni NP structure; *Han et al*. prepared a series of Pd-Ni/SBA-15 bimetallic nanocatalysts with different Pd:Ni ratios: 0.2% Pd – x% Ni/SBA-15, with x = 0.4, 0.7, and 1.2.[35] All bimetallic catalysts had a higher CAL conversion and selectivity to HCAL compared to their monometallic counterparts. The authors attributed these synergistic effects to a better dispersion of Pd in the bimetallic samples. The effects on catalytic performance of Pd-Ni/SBA-15 NPs with a lower Pd content, as studied in this thesis, have not been previously reported.

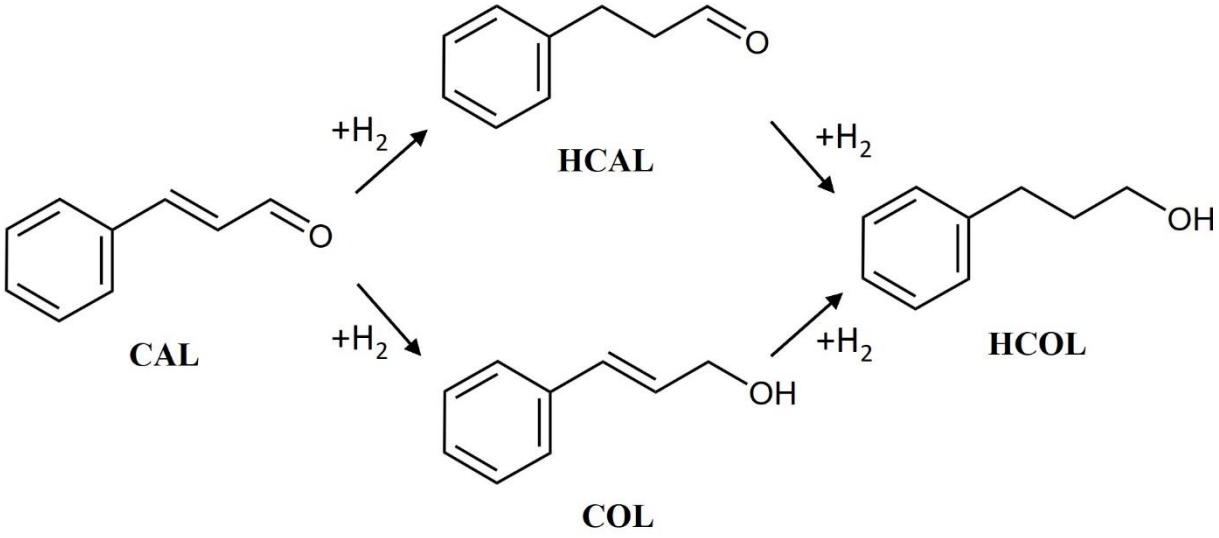

Figure 3. Primary reaction scheme for the selective hydrogenation of cinnamaldehyde (CAL). Three main products can be formed: hydrocinnamaldehyde (HCAL), cinnamic alcohol (COL), and the over-hydrogenated hydrocinnamic alcohol (HCOL).

Citral

The selective hydrogenation of citral is more challenging than the hydrogenation of cinnamaldehyde.[48] Besides a conjugated C=C and C=O bond, citral possesses an additional terpenoid C=C group. This gives rise to many reaction pathways. Figure 4 shows the most relevant ones. The primary products are citronellal and E-Geraniol/Z-Nerol. Citronellol and 3,7-dimethyloctanal can form when more than one unsaturated group is hydrogenated. Palladium and nickel both selectively reduce the conjugated C=C bond, making citronellal the main product.[49] Maximum selectivities similar to in the hydrogenation of CAL have been reported for both metals.[48] *Stolle et al.* studied the effects of Pd-Ni/C composition on citral hydrogenation.[28] To this end, they synthesized bimetallic NPs with (atomic) ratios of Pd:Ni 3:1, 4:1, and 7:1. All bimetallic catalysts were more selective to citronellal compared to Pd/C and showed synergistic activity improvements.

2.2.2 Alkynols

Another important class of selective hydrogenation reactions is the semi-hydrogenation of alkynols to alkenols.[50] This type of transformation is used in the synthesis of fine chemicals

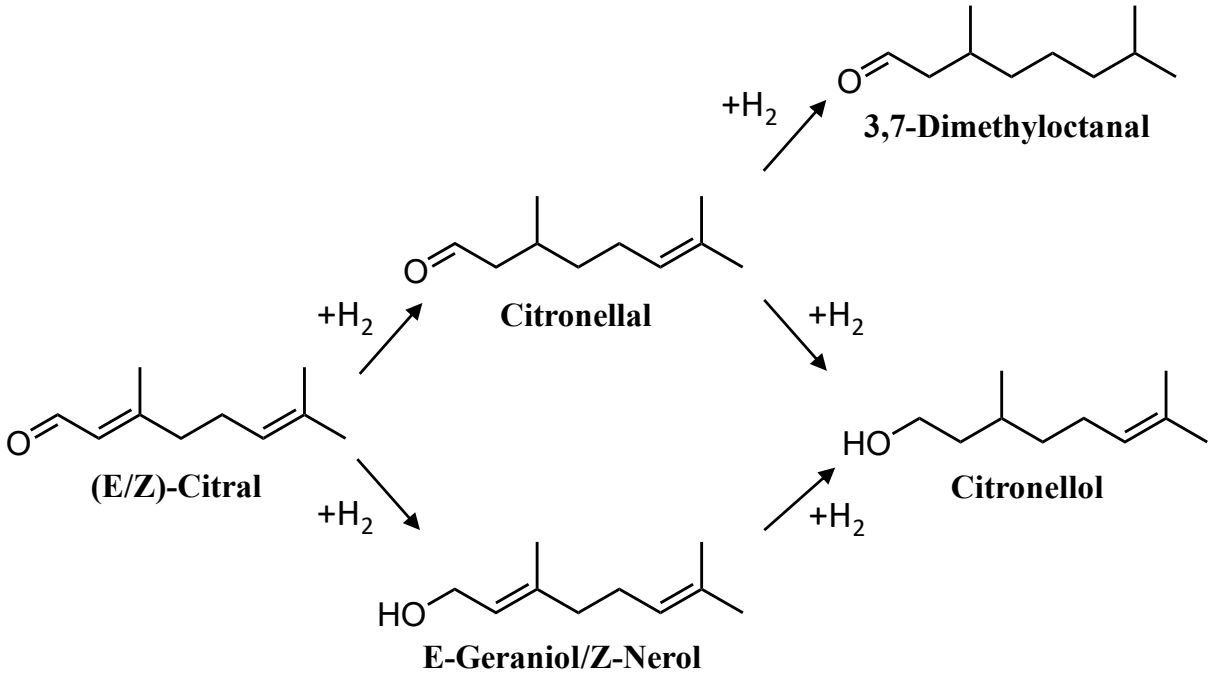

Figure 4. Simplified reaction scheme of the selective hydrogenation of E/Z-citral. The primary products are citronellal and E-geraniol/Z-nerol. Citronellol and 3,7-dimethyloctanal can form when more than one unsaturated group is hydrogenated.

such as vitamins, plastics and agrochemicals. The main challenge is to prevent over-hydrogenation to alkanols and oligomerization.[51] In industry, alkynol hydrogenation reactions are typically catalyzed by the Lindlar catalyst.[50] The Lindlar catalyst (Pd-Pb/$CaCO_3$) is a palladium-based catalyst treated with lead and quinoline to maximize alkenol selectivity. The toxicity of these additives and their adverse effect on activity has sparked a surge of research into alternatives, including supported bimetallic NPs.[50,52]

2-Methyl-3-butyn-2-ol

The industrially relevant semi-hydrogenation of 2-methyl-3-butyn-2-ol (MBY) to 2-methyl-3-buten-2-ol (MBE) is an important model reaction to probe C≡C group selectivity.[50] Figure 5 shows the reaction scheme. The main byproduct is the fully hydrogenated 2-methyl-3-butan-2-ol (MBA). MBA can either form via sequential hydrogenation (MBY → MBE → MBA) or direct hydrogenation (MBY → MBA).[53] The oligomerization of adsorbed alkynol species can produce dimers.[54]

Palladium is among the metals with the highest selectivity to MBE, owing to the higher adsorption strength of the C≡C group compared to the C=C bond.[50] Nickel is considerably less studied in the hydrogenation of MBY, but has shown similar maximum selectivities (over 90%) in the reduction of other alkynols.[51,55] The hydrogenation of MBY is structure sensitive.[56] However, to the best of our knowledge, this has not been studied for Pd-Ni NPs. *González-Fernández et al.* investigated the catalytic performance of Pd-Ni/Al_2O_3 in the gas phase hydrogenation of 3-butyn-2-ol.[36] They reported enhanced Pd-Ni/Al_2O_3 activity and selectivity compared to its monometallic counterparts.

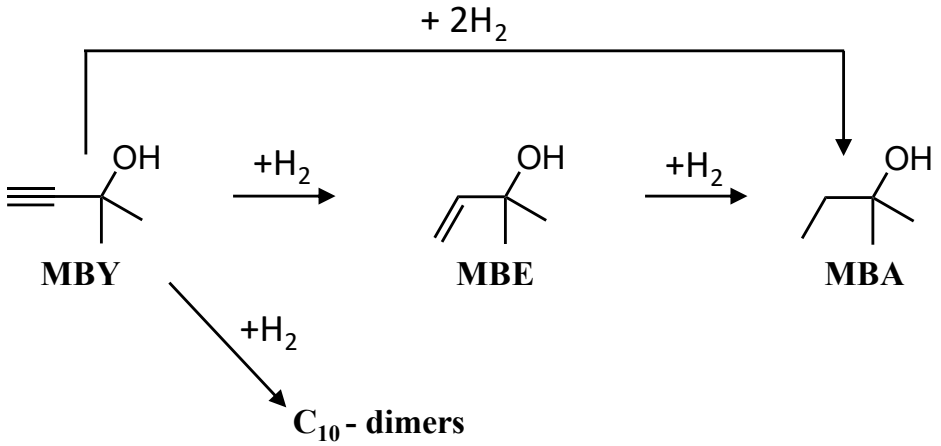

Figure 5. Primary reaction scheme for the hydrogenation of 2-methyl-3-butyn-2-ol (MBY). The main product is 2-methyl-3-buten-2-ol (MBE). 2-Methyl-3-butan-2-ol (MBA) is the over-hydrogenated product, which may form via MBE or directly from MBY. Oligomerization of adsorbed alkynol species can produce dimers.

2.3 Stability

Catalytic performance degrades over time.[57] In liquid phase heterogeneous reactions this may be caused by leaching.[58] Leaching concerns the dissolution of catalyst components into the liquid phase. This negates one of the main advantage of heterogeneous catalysis: easy separation and recovery of the catalyst.[59] In batch reactor systems, the leached metal species remain in the reaction medium. They may, therefore, participate in the reaction, i.e. the reaction is not truly heterogeneous.[60]

The cause of leaching is often difficult to determine, as many factors can play a role.[61] This includes: weak metal-support interactions and high shear forces caused by rapid stirring, metal oxidation; the reaction temperature, pressure, and gas atmosphere; and the interaction of the active sites with the solvent, reactants, intermediates and/or products.[60–63] These have all been reported to play a role in the leaching of Ni and/or Pd species in organic liquid phase (hydrogenation) reactions.[64–68] The stability of bimetallic Pd-Ni NPs is largely unexplored.[69,70] However, accounts on other bimetallic heterogeneous systems have indicated that bimetallic NPs can show a greater resistance to leaching compared to their monometallic counterparts.[71,72]

3

Experimental

3.1 Chemicals

All chemicals were used as received. Trans-Cinnamaldehyde (CAL, 99 %, Sigma-Aldrich), Citral (95 %, Sigma-Aldrich), Ethylenediamine (EDA, 99 %, ACROS), Hydrochloric acid (HCl, 37 wt%, 12.2 M, Merck), Isopropanol (IPA, 99.9 %, Sigma-Aldrich), 2-Methyl-3-butyn-2-ol (MBY, 98 %, Sigma-Aldrich), Nickel(II) nitrate hexahydrate ($Ni(NO_3)_2 \cdot 6H_2O$, 95 %, Sigma-Aldrich), Octane (99 %, Sigma-Aldrich), Palladium(II) Acetate ($Pd(OAc)_2$, 99.9 %, Sigma-Aldrich), Pluronic P123 ($EO_{20}PO_{70}EO_{20}$, Mn∼5,800, Sigma-Aldrich), Tetradecane (99 %, Sigma-Aldrich), Tetraethyl orthosilicate (TEOS, 98 %, Sigma-Aldrich), Toluene (99.85 %, ACROS). All H_2O used in catalyst preparation and testing was of milli-Q grade (deionized, 18.2 MΩ cm).

3.2 Synthesis

3.2.1 Support synthesis

The SBA-15 (887 m^2/g, 1.0 cm^3/g) support was synthesized based on the procedure by *Lee et al.*.[73] First, 23.4 g P123, 607 g H_2O, and 146 g HCL were combined in a 1L polypropylene bottle. The bottle was then heated inside a 55 ˚C oil bath. Magnetic stirring was employed to dissolve all P123. After at least 3 h, the stirring rate was set to 600 rpm and 50 g TEOS was added at once. Exactly 2 minutes later, the stirring bar was removed and the bottle closed. Static conditions were kept for 24 h. Thereafter, the bottle was transferred to a 90 ˚C autoclave oven to allow the silica to condensate for another 24 h. The reaction mixture was then filtered and washed with H_2O until a pH of 5 was reached using a Buchner set-up. After drying the isolated product in a 60 ˚C oven for 4 days, the SBA-15 was calcined in static air at 550 ˚C (1˚C/min) for 6 h.

Table 1. Impregnation parameters used in the preparation of 2 mL precursor solution for the synthesis of bimetallic Pd-Ni/SBA-15 NPs of different Pd:Ni ratios, as well as monometallic reference catalysts.

Sample (Pd:Ni)	Ni wt%	Pd wt%	*x* $Pd(OAc)_2$ (g)	*y* EDA (µL)	*z* H_2O (µL)
Ni	16	x	-	614	948
1:20	16	1.5	0.034	706	925
1:15	16	2.0	0.051	714	918
1:10	16	2.9	0.076	728	903
1:7	16	4.1	0.109	814	1002
Pd	-	3.5	0.076	460	1540

3.2.2 Catalyst preparation

The Pd-Ni NPs of different compositions were prepared by incipient wetness co-impregnation of SBA-15 (887 m^2/g, 1.0 cm^3/g). The following Pd:Ni (atomic) ratios were synthesized: 1:20, 1:15, 1:10, and 1:7, as well as monometallic reference catalysts. The compositional changes were induced by keeping the Ni loading constant (16 wt%), but varying the amount of Pd (1.5 - 4.1 wt%). In a typical synthesis, 2 mL precursor solution was prepared for 0.5 g SBA-15. This called for: 1.022 g $Ni(NO_3) \cdot 6H_2O$, *x* g $Pd(OAc)_2$, *y* µL EDA, and *z* µL H_2O. The amounts of *x*, *y*, and *z* for each sample can be found in Table 1, in addition to the Pd and Ni weight loadings. Before impregnation, the support was dried under static vacuum at 170 ˚C for 1 h. Hereafter, the precursor was contacted with the support under vigorous magnetic stirring. This was done dropwise using a 1 mL syringe. Two impregnation steps were required to achieve the target weight loadings. After each step, the support was dried under vacuum for at least 3 hours. The active phase was obtained by a subsequent calcination and reduction step in a plug flow reactor. All samples were calcined at 450 ˚C for 2 h in air with a heating ramp of 2 ˚C/min and a flow of 300 mL/min · g. Reductions took place under the same conditions, only in an atmosphere of 10 vol.% H_2/N_2 (g). The Ni/SBA-15 catalyst was the only exception and was reduced at 600 ˚C.

3.3 Characterization

3.3.1 Inductively coupled plasma – optical emission spectroscopy

The Pd and Ni weight loadings of fresh and used catalysts were determined with Inductively Coupled Plasma - Optical Emission Spectroscopy (ICP-OES). These measurements were performed by MIKROLAB – Mikroanalytisches Laboratorium Kolbe, Germany. All samples were dried under vacuum at 80 ˚C prior to analysis.

3.3.2 Electron microscopy

Average particle sizes and the dispersion of NPs on the support were investigated with Transmission Electron Microscopy (TEM). To prepare the samples, catalyst powder was dispersed on a Cu grid with a holey carbon Film (Agar, 300). The images were recorded with a Talos F200X microscope operated at 200 kV. Average particle sizes were determined with ImageJ. For this purpose, the diameter of at least 70 particles was measured.

The elemental distribution of Pd, Ni, and Si were mapped using Energy Dispersive X-ray (EDX) spectroscopy measurements. Typically, an acquisition time of 7 minutes and a spot size of 6 was used. The maps were based on net counts averaged over 3 pixels.

3.3.3 Hydrogen temperature-programmed reduction

The reduction behavior of the catalysts (> 150 µm sieve fraction) was analyzed with H_2-Temperature-Programmed reduction (H_2-TPR). The measurements were performed with a Micromeritics AutoChem II Chemisorption Analyzer. First, the samples were dried under Ar atmosphere at 120 ˚C for 1 minute (10 ˚C/min ramp). After allowing them to cool to Room Temperature (RT), the gas flow (25.2 mL STP/min) was changed to 5 vol.% H_2/Ar (g) and the oven set to 600 ˚C (5 ˚C/min ramp). During this step, the hydrogen consumption of the samples was monitored with a Thermal Conductivity Detector (TCD).

3.3.4 Powder X-ray diffraction

Crystal phases were investigated with powder X-Ray Diffraction (XRD) using a Bruker D2 PHASER equipped with a Co (Kα, λ = 1.789Å) X-ray source. The diffractometer was operated at 30 kV and 10 mA. Diffractograms were measured between 15-80˚ 2θ. Only reduced samples were analyzed. To prevent oxidation during the measurements, the XRD samples were prepared under inert atmosphere (Ar) and an airtight dome with built-in scattering screen was placed around the sample holder. Characteristic Ni peaks were identified with an ICDD reference diffractogram: Ni (04-010-6148).

The Scherrer equation was used on the Ni (111) peaks at 51-52˚ 2θ to determine average crystallite sizes (d):

$$d = \frac{K\lambda}{\beta \cos\theta} \quad (1)$$

where K is the dimensionless shape factor, λ the X-ray wavelength (nm), β the Full Width Half Maximum (FWHM) (rad), and θ the Bragg angle (˚). [74] We assumed K = 0.9.

The crystal lattice parameters, a (nm), were calculated with Equation 2 (cubic crystal system) using the same peaks:

$$a = \frac{\lambda}{2 \cdot \sin(\theta)} \sqrt{h^2 + k^2 + l^2} \quad (2)$$

where h, k, and l are the miller indices of the Ni (111) plane, i.e. h = 1, k = 1, and l = 1.[75] The SiO_2 peak of the Ni/SBA-15 catalyst at 26.7˚ 2θ was taken as a reference signal to correct for the experimental peak shift of all catalysts.

The found lattice parameters were compared against the theoretical Vegard's law. The following ICDD reference diffractograms were used to determine the linear relationship between the composition and the lattice parameter of Pd-Ni alloys: Ni (04-010-6148) and $Ni_{0.5252}Pd_{0.475}$ (05-065-5788).

3.3.5 Nitrogen physisorption

The specific surface area and pore volume of the SBA-15 support were analyzed with N_2 physisorption. First, the support was dried under vacuum at 200 °C. Isotherms were then measured at -196 ˚C with a Micrometrics TriStar 3000.

3.4 Catalytic testing

3.4.1 Cinnamaldehyde hydrogenation

The selective hydrogenation of CAL was performed in a 300 mL stainless steel Parr Instrument Company autoclave equipped with a glass liner, sample port, External Catalyst Addition Device (XCAD), mechanical stirrer, and with two gas inlets – one for the reactor and one for the XCAD – that also served as vents. The set-up is depicted in Figure 6. The reduced catalyst samples (25 mg, 75-150 µm sieve fraction) were loaded in the XCAD under inert atmosphere to prevent oxidation. In a typical run, 2.0 g CAL, 2.0 mL H_2O (to prevent acetal formation), 1.0 mL tetradecane (internal standard), and 100 mL IPA (solvent) were combined in the glass liner. After flushing the reactor with N_2 (g) and H_2 (g), the catalyst was added via the XCAD. The reaction mixture was then heated to 80 ˚C under 30 bar H_2 (g) while stirring at 800 rpm. These conditions were kept for the duration of the experiment. Liquid samples (approximately 1.7 mL) were taken from the reaction mixture at given intervals in time. The moment the reaction mixture reached 80 ˚C was defined as t_0. The composition of the extracts was analyzed with a Bruker 550-GC gas chromatograph (GC). To enable the characterization of used catalysts, the entire reaction mixture was filtered (Buchner set-up) after each run.

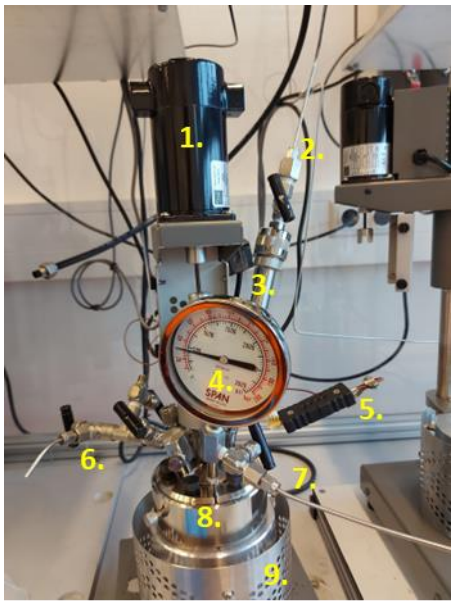

Figure 6. Liquid phase hydrogenation set-up with: 1) mechanical stirrer, 2) XCAD gas inlet/vent, 3) XCAD, 4) pressure gauge, 5) thermocouple, 6) sample port, 7) autoclave gas inlet/vent, 8) autoclave, and 9) heating mantle.

Table 2. Amount of catalyst (75-150 µm sieve fraction) and Pd and Ni (mg) as used for the hydrogenation of citral and MBY.

Sample (Pd:Ni)	Catalyst (mg)	Ni (mg)	Pd (mg)
Ni	35	5.8	-
1:20	35	5.7	0.51
1:15	23	3.8	0.51
1:10	18	2.9	0.51
1:7	10	1.6	0.51
Pd	15	-	0.51

3.4.2 Citral hydrogenation

The same general procedure as for the hydrogenation of CAL was employed. In a typical run, the following was added to the glass liner: 1.8 g citral, 0.5 mL tetradecane, and 120 mL IPA. The catalytic tests were performed at 60 ˚C and 30 bar H_2 (g) with a stirring speed of 800 rpm. For this reaction, the amount of Pd is each run was kept constant instead of the amount of catalyst. Table 2 shows the amounts of catalyst and metal tested for each sample.

Note: blank runs (only reactant, no catalyst) were performed before transitioning to a new reaction. This was done to ensure there was no conversion by leached species or remaining catalyst from the previous runs.

3.4.3 2-Methyl-3-butyn-2-ol hydrogenation

A minor adjustment to the catalytic testing protocol was made: the reaction mixture was heated to the desired temperature under inert atmosphere (N_2 (g)). After allowing the temperature to stabilize, the gas atmosphere was changed to H_2 (g). This moment was defined as t_0. The following was added to the glass liner: 2.3 g MBY, 0.5 mL octane (internal standard), and 120 mL toluene (solvent). The hydrogenation of MBY was executed at 50 ˚C and 30 bar H_2 (g) while stirring at 800 rpm. The same amounts of catalysts were used for this reaction as in the hydrogenation of citral (Table 2).

3.4.4 Calculations

The activity, conversion, and selectivity of each catalyst were calculated based on the concentration of the reactant and the products in the samples extracted from the reaction mixture over time. These concentrations were quantified with GC (see 3.4.1).

Conversion
The conversion, X (%), of the reactant (CAL, citral, or MBY) was determined using the following equation:

$$X_{reactant} = \frac{N_{reactant,t_0} - N_{reactant,t_i}}{N_{reactant,t_0}} \times 100\ \% \quad (3)$$

where $N_{reactant}$ represents the moles of reactant at reaction time i.

Selectivity

Equation 4 was used to calculate the selectivity, S (%), to the main product:

$$S = \frac{N_{main\ product,t_i}}{N_{all\ products}} \times 100\ \% \quad (4)$$

In this formula, $N_{main\ product}$ stands for the moles of main product at reaction time i. The main product is hydrocinnamaldehyde (CAL hydrogenation), citronellal (citral hydrogenation), or 2-methyl-3-buten-2-ol (MBY hydrogenation). The term $N_{all\ products}$ is a summation of the moles of all products at reaction time i. These are:

- CAL hydrogenation: hydrocinnamaldehyde (HCAL), cinnamic alcohol (COL), and hydrocinnamic alcohol (HCOL).
- Citral hydrogenation: citronellal, citronellol, and 3,7-dimethyloctanal.
- MBY hydrogenation: 2-methyl-3-buten-2-ol (MBE), and 2-methyl-3-butan-2-ol (MBA).

Turnover frequency

Apparent turnover frequencies (TOFs) were determined using the following equation:

$$TOF = \frac{k}{N_{surface\ metal}} \quad (5)$$

where k is the intrinsic reaction rate and $N_{surface\ metal}$ the moles of surface metal of the supported NPs. For the hydrogenation of CAL and citral, a 1st order rate dependency on the reactant concentration was assumed. Hence, k (1/s) was determined from the slope of a linear fit in a logarithmic reactant concentration (M) versus time (s) plot. For the hydrogenation of MBY, a 0th order dependency of the reaction rate on the reactant concentration was assumed. Therefore, k (M/s) was the slope of a linear fit in a concentration (M) versus time (s) plot. Reactant concentrations up to a maximum of 90 % conversion were included in all plots.

Equation 6 was used to determine $N_{surface\ metal}$. This formula was based on the metal dispersion of Pd NPs. We assumed it would resemble the metal dispersion of Pd-Ni NPs.

$$N_{surface\ metal} = \frac{1.122}{d_{NP}} \quad (6)$$

The average NP diameter obtained with TEM analysis is expressed as d_{NP} (nm).

4

Results and Discussion

4.1 Characterization

In this work, we synthesized Pd/SBA-15, Ni/SBA-15, and Pd-Ni/SBA-15 model catalysts of different compositions by incipient wetness (co-)impregnation of SBA-15. The amount of Pd precursor salt was varied to obtain bimetallic NPs of 16 wt% Ni and 1.5-4.1 wt% Pd. This corresponds to the following Pd:Ni (atomic) ratios: 1:20, 1:15, 1:10, and 1:7. We performed ICP-OES on the Pd-Ni/SBA-15 catalysts and their monometallic counterparts to establish if the target weight loadings and ratios were achieved. The results, presented in Table 3, confirm for each sample that the desired amounts of Pd and Ni are on the support. While all weight loading are slightly below the theoretical values, they meet expectations. The deviations from theory are likely the result of e.g. impurities in the precursor salts and/or not all precursor winding up on the support (but on the glassware/stirring bar instead).

The dispersion of NPs and the elemental distribution of Pd and Ni on the support were investigated with HAADF STEM(-EDX). Figure 7 provides an overview of the obtained Pd-Ni/SBA-15 images (see Appendix A for the monometallic reference catalysts). Images A1-D1 reveal a homogeneous dispersion of the NPs with average diameters of 3.6-3.8 ± 0.8 nm. The elemental maps of Ni (red) and Pd (green) (and Si in blue) in images A2-D2/A3-D3 show an even distribution of both metals. Overlapping EDX signals suggest intimacy between Ni and Pd and bimetallic particles. A few monometallic Pd clusters are observed for the Pd-Ni/SBA-15 catalyst with the highest Pd content (Pd:Ni 1:7) (not shown here).

Table 3. Metal weight loadings (Pd and Ni) and atomic Pd:Ni ratios of Ni/SBA-15, Pd/SBA-15, and Pd-Ni/SBA-15 catalysts based on theory and ICP-OES measurements.

Theoretical Ratio (Pd:Ni)	ICP Ratio (Pd:Ni)	Theoretical Ni wt%	ICP Ni wt%	Theoretical Pd wt%	ICP Pd wt%
Ni	Ni	16	16.04	x	x
1:20	1:20.6	16	14.06	1.5	1.24
1:15	1:15.0	16	13.05	2.0	1.58
1:10	1:9.5	16	14.61	2.9	2.78
1:7	1:7.0	16	12.92	4.1	3.34
Pd	Pd	x	x	3.5	3.32

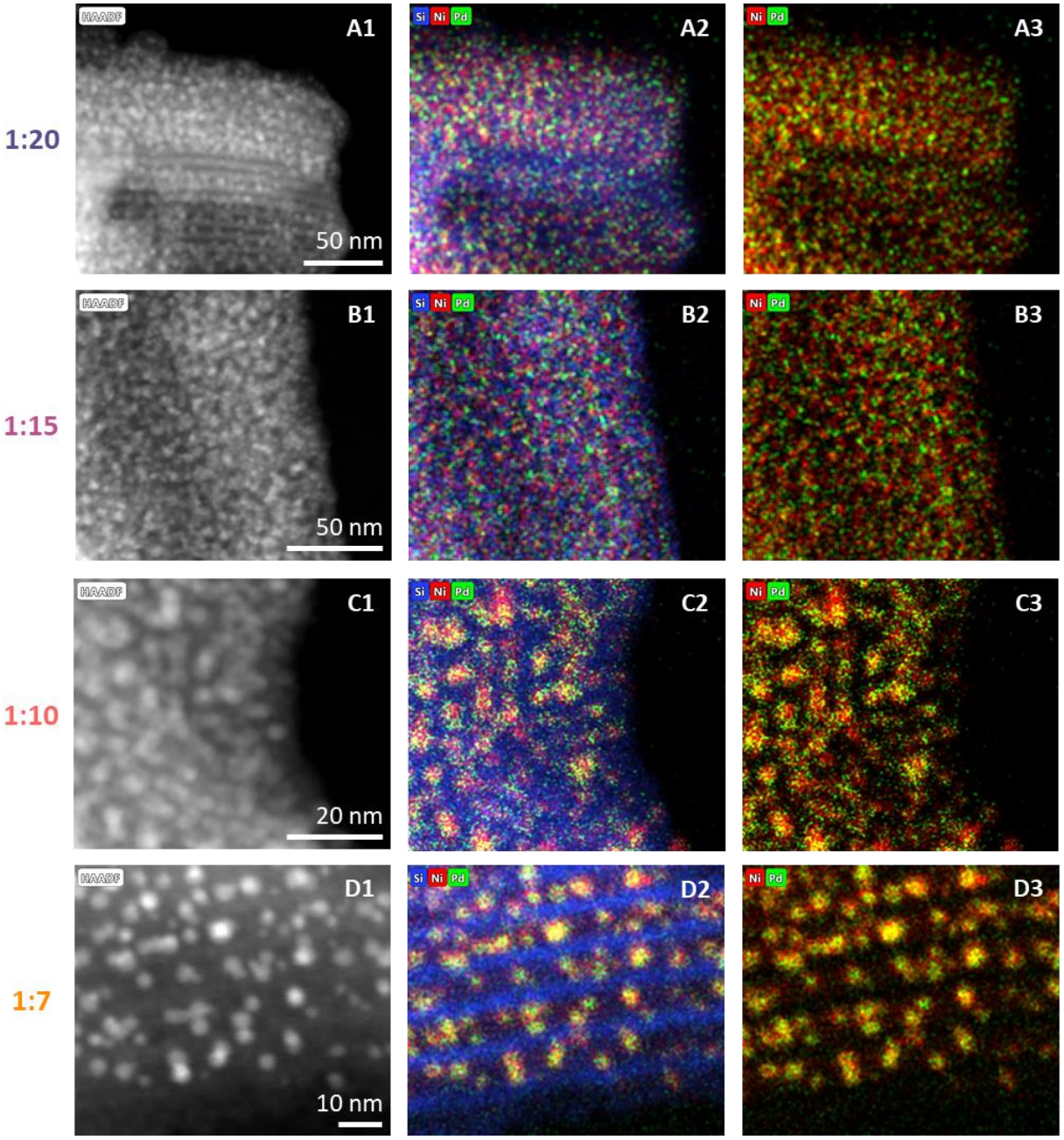

Figure 7. HAADF STEM images (A1-D1) and EDX maps (A2-D2/A3-D3) of Pd-Ni/SBA-15 catalysts with NPs of different Pd:Ni ratios.

Metallic palladium can promote the reduction of nickel oxide via hydrogen spillover from dissociative adsorption of H_2 (g).[76,77] This is a proximity effect.[78] Hence, H_2-TPR was used as a bulk technique to probe the intimacy of Pd an Ni. The H_2-TPR profiles of Ni/SBA-15 and all Pd-Ni/SBA-15 catalysts are plotted in Figure 8. The Pd/SBA-15 catalyst was not measured, as Pd typically reduces at room temperature.[79] The peaks in H_2 consumption of all presented samples are therefore attributed to the reduction of $Ni^{2+} \rightarrow Ni^0$. The Ni/SBA-15 catalyst shows a maximum at 550 ˚C. Its broad signal suggests the reduction of several nickel oxide species. The peak positions of the bimetallic catalysts are shifted to lower temperatures by approximately 300 ˚C. This, together with the homogeneity in their peak shapes, indicates a similar and close proximity of Pd an Ni for all Pd:Ni ratios.

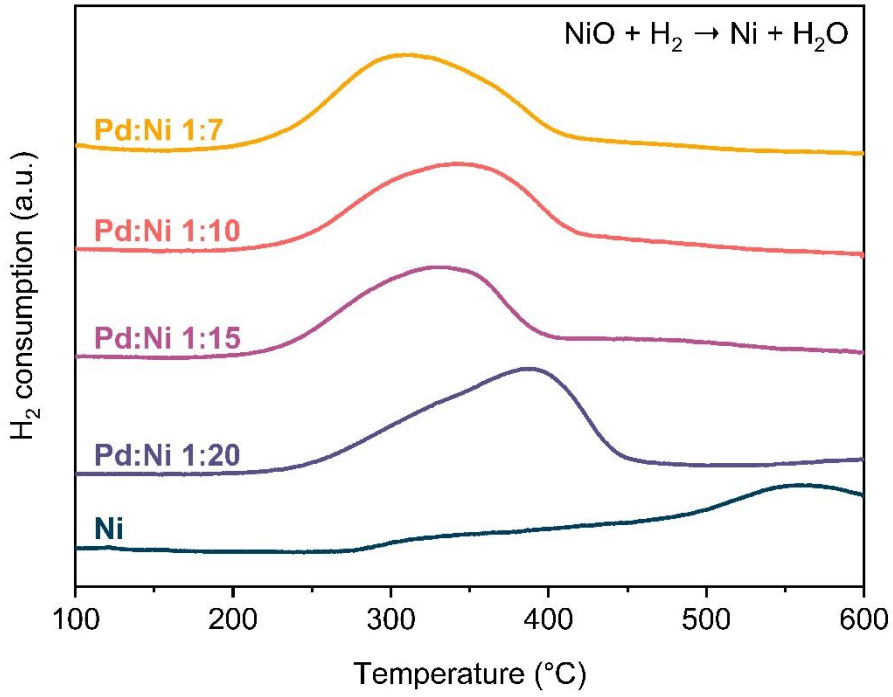

Figure 8. H_2-TPR profiles of Ni/SBA-15 and Pd-Ni/SBA-15 NPs with different Pd:Ni atomic ratios.

Powder XRD patterns were obtained to determine if the bimetallic NPs are alloyed. Reduced samples were measured under inert atmosphere. Figure 9A shows the diffractograms of Ni/SBA-15 and every Pd-Ni/SBA-15 catalyst. The Pd/SBA-15 NPs were not measured for XRD due to their small size (d = 1.5 ± 0.5 nm). Three distinct signals are identified for the other catalysts. The signals at 26.7˚ 2θ corresponds to the support (SiO_2). The broad peaks suggests short range order. Signals at 51.2-51.7˚ and 59.8-60.8˚ 2θ are assigned to the Ni (111) and Ni (200) planes, respectively. This is characteristic of a face centered cubic (FCC) structure.[75] Compared to Ni/SBA-15, the positions of the Pd-Ni/SBA-15 Ni (111) and Ni (200) planes are shifted to lower Bragg angles. This indicates the incorporation of Pd inside the Ni crystals in

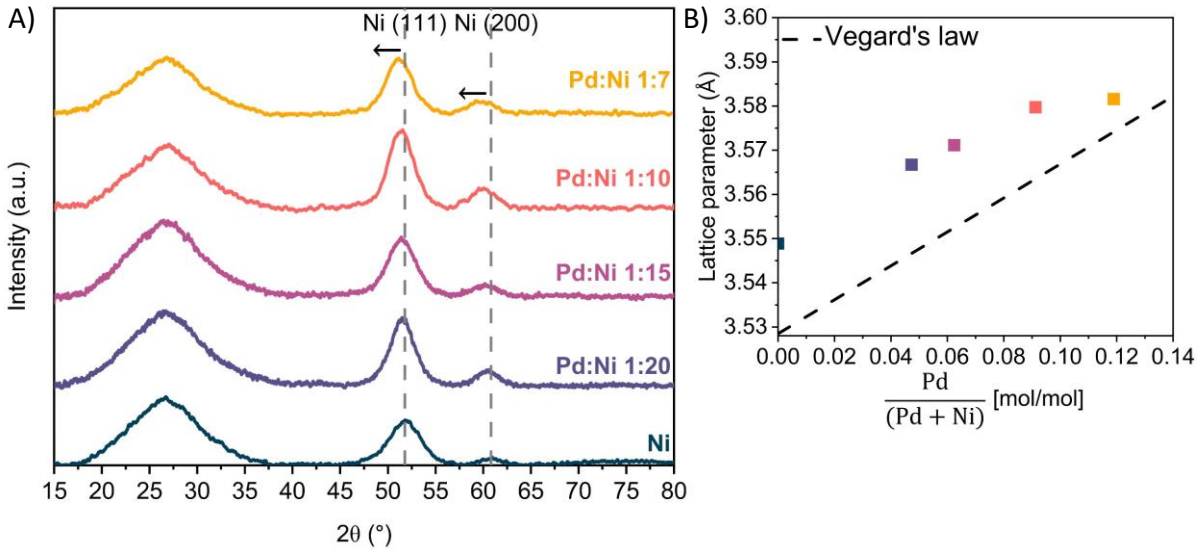

Figure 9. A) XRD patterns of Ni/SBA-15 and Pd-Ni/SBA-15 NPs with different Pd:Ni ratios. B) Lattice parameter plotted against the Pd content of the Ni/SBA-15 and Pd-Ni/SBA-15 catalysts. The dashed line represents the theoretical Vegard's law.

an alloyed phase. As the atomic radius of Pd (169 pm) is larger than that of Ni (149 pm), Pd expands the Ni FCC lattice.[36,80] This is observed as a peak shift to lower angles.

According to Vegard's law, the lattice expansion should scale linearly with the composition of alloyed NPs.[20] Therefore, to determine if the bimetallic NPs are of the intended compositions, the lattice parameters of the Ni/SBA-15 and the Pd-Ni/SBA-15 catalysts were calculated. The results are plotted in Figure 9B. The dashed line represents the theoretical Vegard's law, which was based on a Ni and Pd-Ni reference diffractogram (see 3.3.4). The lattice parameters of the bimetallic catalysts show only a minimal deviation from theory (0.02 Å). More importantly, they scale linearly with an increasing Pd content and the slope is consistent with Vegard's law. This suggests that Pd is incorporated in the Ni crystal domains in accordance with the Pd:Ni ratio. The only exception is the Pd-Ni/SBA-15 1:7 catalyst. Its lattice parameter is smaller than expected based on the linear trend the other bimetallic NPs follow. This is likely due to the monometallic Pd clusters in this catalyst, as observed with TEM.

The average crystallite sizes of the NPs in each catalyst were determined by using the Scherrer equation on the Ni (111) signals. Table 4 shows the results in addition to the average particle sizes found with TEM. The finding from the XRD data confirm what TEM analysis already indicated: the Ni/SBA-15 and all Pd-Ni/SBA-15 NPs are uniform in size. Only the Pd/SBA-15 NPs are smaller. This is likely caused by its lower metal weight loading (3.3 wt%).

Thus far, the HAADF STEM(-EDX), H_2-TPR and XRD results demonstrate the successful synthesis of uniformly sized Pd-Ni/SBA-15 catalysts with the intended Pd:Ni ratios. As all catalysts only considerably vary in NP composition and not size, it is possible to determine structure-performance relationships based on composition. For this purpose, the model catalysts were investigated for the liquid phase selective hydrogenation of: 1) cinnamaldehyde (section 4.2), 2) citral (section 4.3), and 3) 2-methyl-3-butyn-2-ol (section 4.4).

Table 4. Average crystallite and NP sizes of the Pd/SBA-15, Ni/SBA-15, and Pd-Ni/SBA-15 NPs with different Pd:Ni ratios based on XRD and TEM analysis, respectively.

Sample (Pd:Ni)	XRD Crystallite size (nm)	TEM Particle size (nm)
Ni	2.5	3.1 ± 0.8
1:20	3.3	3.8 ± 0.9
1:15	3.0	3.6 ± 0.8
1:10	3.2	3.7 ± 0.8
1:7	3.1	3.8 ± 1.1
Pd	-	1.5 ± 0.5

4.2 Cinnamaldehyde hydrogenation

In the hydrogenation of cinnamaldehyde (CAL), the activity of the Pd/SBA-15, Ni/SBA-15 and Pd-Ni/SBA-15 catalysts varies with composition. Figure 10 shows the activity as a function of the Pd content. The catalytic activity is expressed as the apparent turnover frequency (TOF in s^{-1} mol surface $metal^{-1}$). These values were determined using the intrinsic reaction rate assuming first order CAL conversion. The dashed line is a guide to the eye and represents an additive relationship between the Pd content and the TOF. As expected, the Pd/SBA-15 catalyst is considerably more active than Ni/SBA-15. The activity of the bimetallic NPs is also higher than

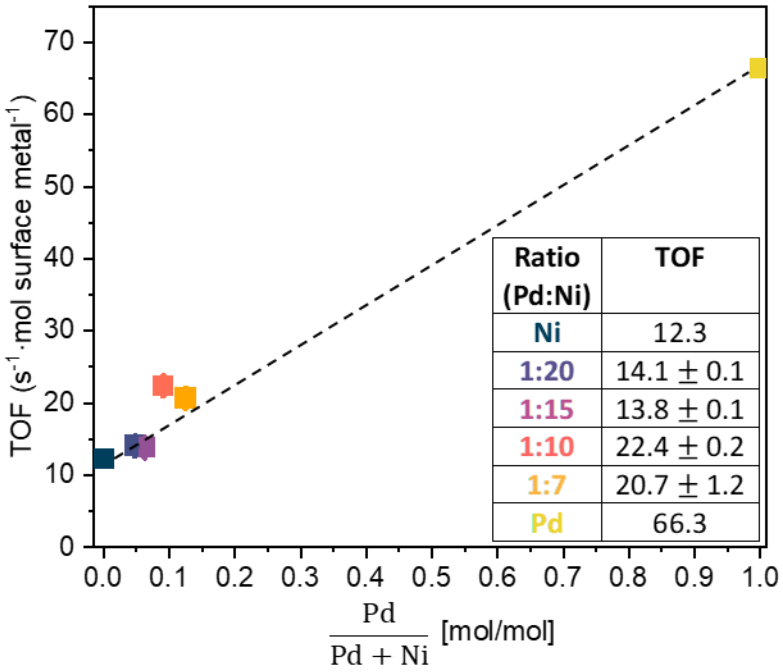

Figure 10. Apparent turnover frequencies (TOFs) of Pd/SBA-15, Ni/SBA-15, and Pd-Ni/SBA-15 catalysts with different Pd:Ni atomic ratios in the selective hydrogenation of cinnamaldehyde (CAL). The TOFs are plotted against the Pd content of the NPs. The dashed line is a guide to the eye that represents an additive relationship between the Pd content and the activity. Conditions: 80 ˚C, 30 bar H_2 (g), 800 rpm stirring rate, 147 mM CAL in 2-propanol, 25 mg catalyst.

that of Ni/SBA-15 and increases with an increasing Pd concentration. The small differences in composition and the method employed to determine the reaction rate (using a fit) make it difficult to establish a trend between the TOF of the Pd-Ni/SBA-15 NPs and their Pd content. However, their TOFs lie close to the dashed line in the figure. Palladium may thus have an additive effect on the activity of the bimetallic catalysts.

The conversion of CAL and the formation of the products (HCAL, COL, and HCOL) were monitored over time. This is shown in Figure 11 for the Pd/SBA-15, Ni/SBA-15 and Pd-Ni/SBA-15 Pd:Ni 1:10 catalysts. The reaction profile of the 1:10 sample is representative for all bimetallic ratios (Appendix B). In agreement with literature, each catalyst forms HCAL as their main product, followed by HCOL.[46] Almost no COL is observed. Palladium and Ni both favor C=C bond hydrogenation. Any COL that forms is thus likely almost immediately converted to HCOL.[46] Distinct is the relative amount of HCOL for the Pd/SBA-15, Ni/SBA-15, and Pd-Ni/SBA-15 catalysts at every level of CAL conversion. The following general trend is observed: Pd/SBA-15 > Pd-Ni/SBA-15 > Ni/SBA-15. These findings indicate that incorporating dilute amounts of Pd in Ni NPs reduces the selectivity to the C=C bond. As discussed in Chapter 2, the selectivity is largely governed by the metal d-band width of the catalyst.[43] Because Pd has a broader d-band that Ni, adding Pd to Ni/SBA-15 expands the d-band. This increases the repulsive interaction between the C=C bond and the NPs.[81] Consequently, the bimetallic NPs are more likely to adsorb CAL top-on, thereby promoting C=O bond hydrogenation/HCOL formation.

Based on the aforementioned theory and observations, the selectivity to the main product (HCAL) should follow the opposite trend to the relative concentration of HCOL, i.e. Ni/SBA-

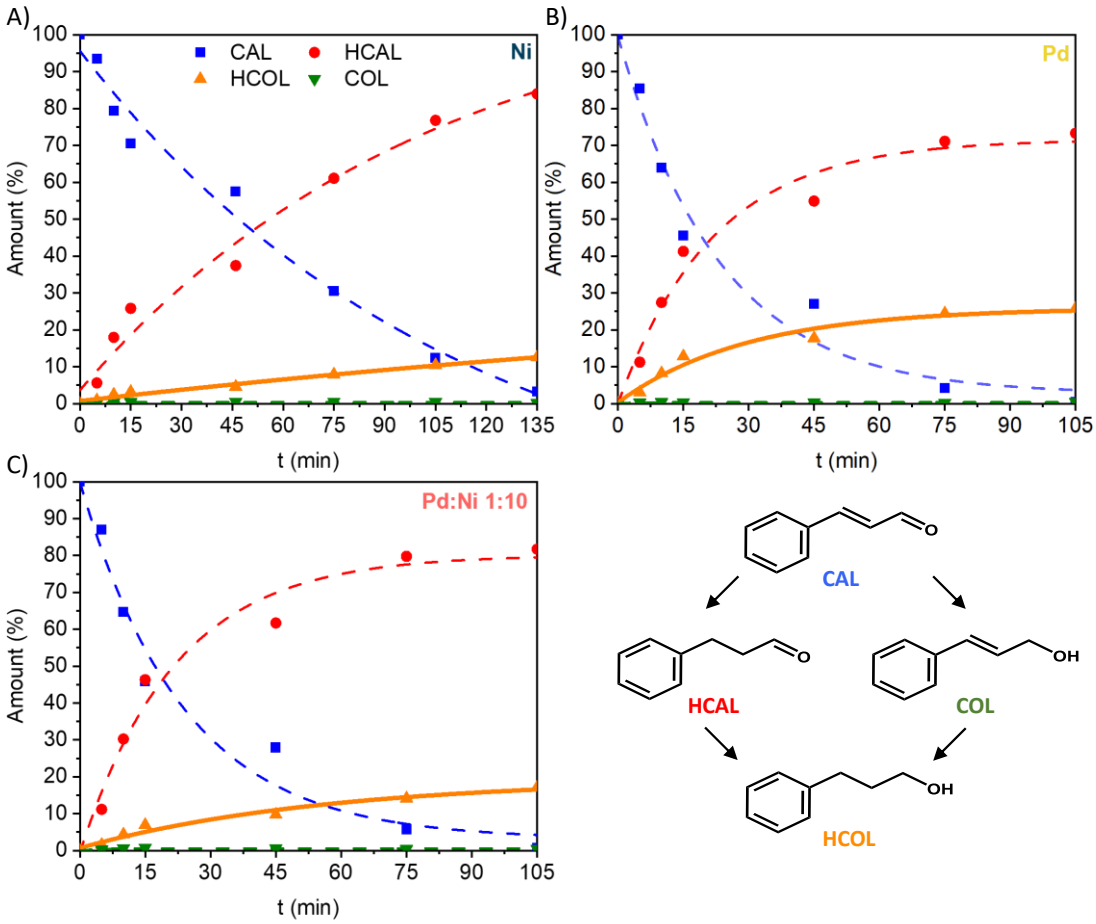

Figure 11. Relative amounts of cinnamaldehyde (CAL), hydrocinnamaldehyde (HCAL), cinnamic alcohol (COL), and hydrocinnamic alcohol (HCOL) during the selective hydrogenation of CAL, catalyzed by A) Ni/SBA-15, B) Pd/SBA-15, and C) Pd-Ni/SBA-15 Pd:Ni 1:10. Conditions: 80 ˚C, 30 bar H_2 (g), 800 rpm stirring rate, 147 mM CAL in 2-propanol, 25 mg catalyst.

15 > Pd-Ni/SBA-15 > Pd/SBA-15. This is confirmed in Figure 12, which depicts the selectivity to HCAL against the CAL conversion for each catalyst. However, no relationship between the HCAL selectivity of the Pd-Ni/SBA-15 catalysts and the Pd content is observed. As all NPs are similar in composition, their selectivity could lie within each other's experimental error.

Together, the results in Figure 11 and 12 show that the activity of the Pd-Ni/SBA-15 NPs increases with the Pd content. Yet while their selectivity to HCAL is slightly reduced compared to Ni/SBA-15, it remains similar. This may be explained by the following mechanism; the reactant is mainly adsorbed by the nickel atoms. Palladium then increases the reaction rate by providing extra hydrogen via spillover, as observed with H_2-TPR.

Our findings are in disagreement with Han et al. (section 2.3.1), who observed a synergistic selectivity of their Pd-Ni/SBA-15 catalysts in the hydrogenation of CAL.[35] However, their Ni/SBA-15 catalyst had a 14% selectivity to HCAL (at 29% CAL conversion). This is considerably lower than reported here and in other sources.[46] The bimetallic catalysts of *Han et al.* have a similar HCAL selectivity to the Pd-Ni/SBA-15 NPs in this work (around 85%).

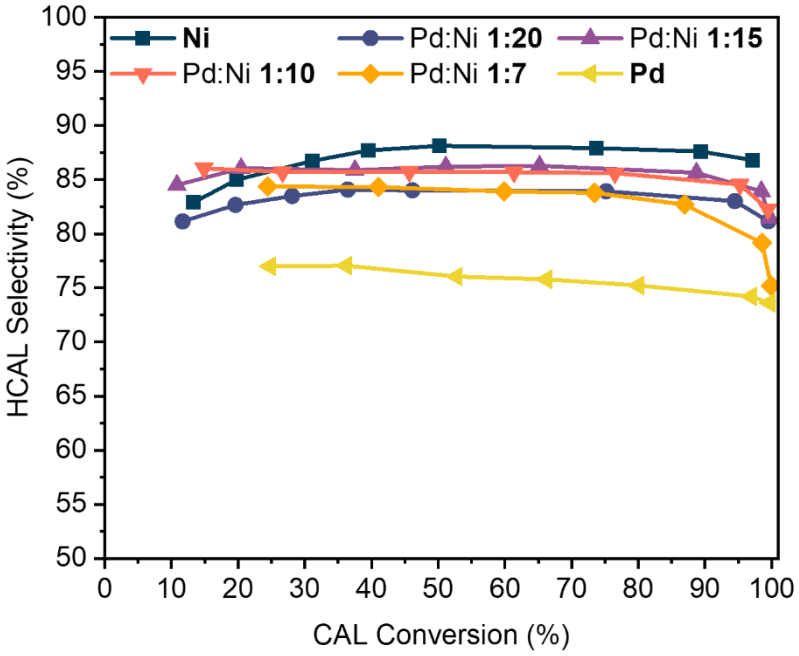

Figure 12. Hydrocinnamaldehyde (HCAL) selectivity as a function of the cinnamaldehyde (CAL) conversion in the hydrogenation of CAL for Pd/SBA-15, Ni/SBA-15, and Pd-Ni/SBA-15 catalysts with different Pd:Ni ratios. Conditions: 80 ˚C, 30 bar H_2 (g), 800 rpm stirring rate, 147 mM CAL in 2-propanol, 25 mg catalyst.

After the reaction, all catalysts were investigated with electron microscopy to study their stability. HAADF STEM(-EDX) analysis of used Pd/SBA-15 and Pd-Ni/SBA-15 catalysts reveals leached metal species, as depicted in Figure 13 (only Pd:Ni 1:10 shown). No leaching is observed for Ni/SBA-15. The pores of the Pd/SBA-15 catalyst appear almost empty and large agglomerates are outside of the support. It is unknown whether these structures form on the TEM grid or during the reaction. In contrast, the Pd-Ni/SBA-15 catalysts seem considerably more stable; most NPs are still inside the support. No changes in the average particle sizes are observed. The EDX maps of the used bimetallic catalysts imply that the leached species are monometallic, as shown in the figure for the Pd:Ni 1:10 catalyst. The structure of the NPs inside the support appears unaltered (EDX maps not shown).

The leached species may have been active during the reaction. CAL conversion was observed in blank runs (only reactant, no catalyst) between tests. Leached metals could have remained inside the reactor system after cleaning. However, at which point during the reaction leaching

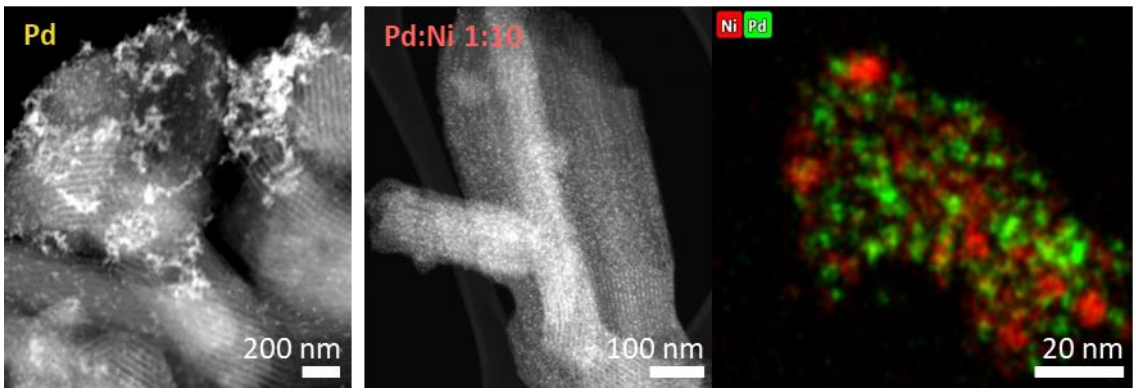

Figure 13. HAADF STEM images and an EDX map of a used Pd/SBA-15 (left) and Pd-Ni/SBA-15 Pd:Ni 1:10 (middle and right) catalyst after the hydrogenation of cinnamaldehyde.

Table 5. Comparison of the Pd:Ni ratios and Pd and Ni weight loadings of fresh and used Pd/SBA-15 and Pd-Ni/SBA-15 catalysts tested for the hydrogenation of cinnamaldehyde.

Fresh **Ratio (Pd:Ni)**	Used **Ratio (Pd:Ni)**	Fresh vs Used **% decrease Pd**	Fresh vs Used **% decrease Ni**
1:20.6	1:19.1	+9.7	+1.7
1:9.5	1:9.5	-10.8	-10.2
Pd	Pd	-41.6	-

occurs and to what extent leached metal species participate in the actual catalytic runs remains to be investigated.

To validate the observations made with TEM, fresh and used catalysts (Pd/SBA-15, Pd-Ni/SBA-15 Pd:Ni 1:20 and 1:10) were also investigated with ICP-OES. Table 5 shows the results. Relatively less Pd is leached from the bimetallic catalysts compared to Pd/SBA-15. These findings further indicate that the bimetallic catalysts show a greater resistance to leaching compared to Pd/SBA-15. Furthermore, the Pd:Ni ratios of the used Pd-Ni/SBA-15 catalysts resemble the ratio of their fresh counterpart. This implies that, despite moderate leaching, the NPs remain of the intended composition for the duration of the reaction. Curiously, the used Pd:Ni 1:20 catalyst has a higher metal loading after catalysis compared to before. This is probably due to inaccurate ICP-OES results, caused by e.g. inhomogeneities in the samples (at most a few milligrams were used for ICP-OES) or the loss of SBA-15 during the reaction.

4.3 Citral hydrogenation

The previous section showed that incorporating dilute amount of Pd in Ni/SBA-15 NPs can be a way to maintain a similarly high selectivity to the C=C bond as the monometallic Ni catalyst, while making effective use of the highly active Pd. However, the differences in activity and selectivity between the bimetallic catalysts were small and sometimes inconclusive. Compared to CAL, Citral is a less rigid compound with an additional terpene moiety. The hydrogenation of Citral might therefore be more structure sensitive.

The TOFs (s^{-1} · mol surface $metal^{-1}$) of the Ni/SBA-15, Pd/SBA-15, and Pd-Ni/SBA-15 catalysts are plotted against their Pd content in Figure 14. In this reaction, the activity of the Pd-Ni/SBA-15 NPs is considerably more sensitive to the NP composition. However, unlike in the hydrogenation of CAL, all bimetallic catalysts are less active than their monometallic counterparts. Moreover, their TOF drops with an increasing Pd content. The reason behind this observation remains speculative. To confirm if the alloying of Pd and Ni is responsible, a catalyst with Pd and Ni in separate phases (Pd+Ni/SBA-15, Pd:Ni 1:10) was also tested for the hydrogenation of citral. The results are in Appendix C. The TOF of the Pd+Ni/SBA-15 NPs is considerably higher than that of its alloyed counterpart. These findings suggest that the electronic and/or geometric changes as a result of alloying are (largely) responsible for the decreased activity of the bimetallic catalysts. In literature, deactivation of Pt-group metals in citral hydrogenation is often ascribed to active site poisoning due to strongly adsorbed CO or hydrocarbon fragments.[82,83] We, therefore, propose than an increasing Pd content changes the electronic and/or geometric properties of the Pd-Ni/SBA-15 NPs in such a way, that the C=O and/or C=C groups of citral or its products adsorb more strongly to the catalyst surface with higher Pd concentrations. Curiously, no deactivation was observed in the hydrogenation of

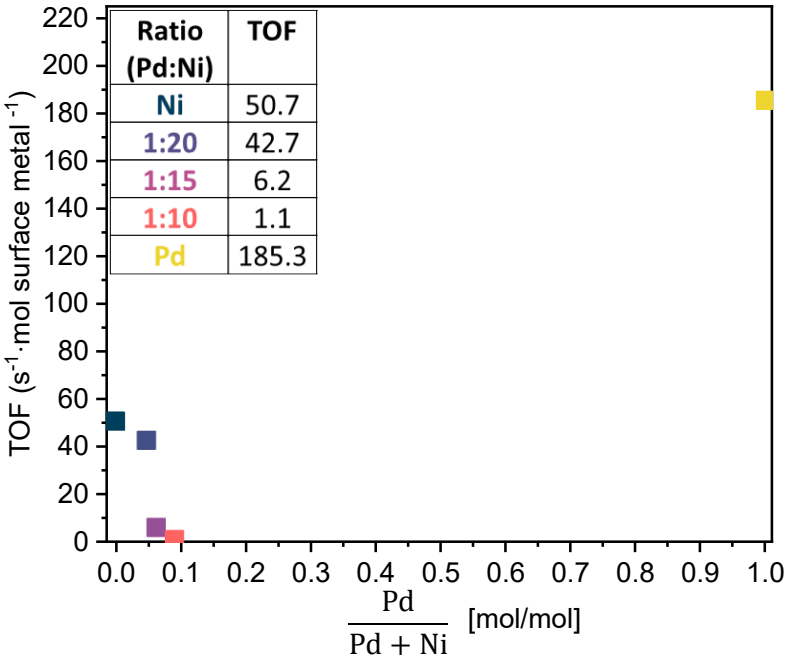

Figure 14. Apparent turnover frequencies (TOFs) of Pd/SBA-15, Ni/SBA-15, and Pd-Ni/SBA-15 catalysts with different Pd:Ni atomic ratios in the selective hydrogenation of citral. The TOFs are plotted against the Pd content of the NPs. Conditions: 60 ˚C, 30 bar H_2 (g), 800 rpm stirring rate, 96 mM citral in 2-propanol, 10-35 mg catalyst (0.5 mg Pd).

CAL. A possible explanation might be that the higher flexibility of citral results in a different interaction with the active sites compared to CAL.

The composition of the reaction mixture was monitored over time. This is shown in Figure 15A-C for Pd/SBA-15, Ni/SBA-15 and Pd-Ni/SBA-15 1:20 (see Appendix D for the other ratios). As expected, all catalysts form citronellal as their main product. Two other products are identified: citronellol and 3,7-dimethyloctanal. The relative concentrations of the products are distinct at each level of citral conversion for Pd/SBA-15, Ni/SBA-15 and the bimetallic catalysts. Based on this, a general reaction pathway for the different samples was established. This is depicted in Figure 15D. The Ni/SBA-15 catalyst shows a decrease in the amount of citronellal at approximately 85% (when almost no citral is left). This drop is proportional to the increase in citronellol, indicating citronellal to citronellol conversion. The direct conversion of citronellal to citronellol by nickel is described in literature.[48] In contrast, almost no citronellol is formed by Pd/SBA-15. However, this catalyst forms considerably more 3,7-dimethyloctanal. The reaction profile of the bimetallic catalyst shows the influence of both its constituent metals; the Pd-Ni/SBA-15 NPs generate less citronellol than Ni/SBA-15, but more 3,7-dimethyloctanal at similar levels of citral conversion.

Figure 16 displays the selectivity to the main product (citronellal) against the citral conversion. The same general trend as in the hydrogenation of CAL is observed: Ni/SBA-15 is the most selective, Pd/SBA-15 the least, and the Pd-Ni/SBA-15 catalysts are almost as selective as the Ni NPs. No trend in the Pd content of the Pd-Ni/SBA-15 catalysts and their selectivity to the main product is found. This may be explained by the same reason as in the hydrogenation of CAL.

HAADF STEM(-EDX) analysis of used catalysts reveals similar leaching behavior to in the hydrogenation of CAL. However, while only a few EDX maps were collected, they indicate

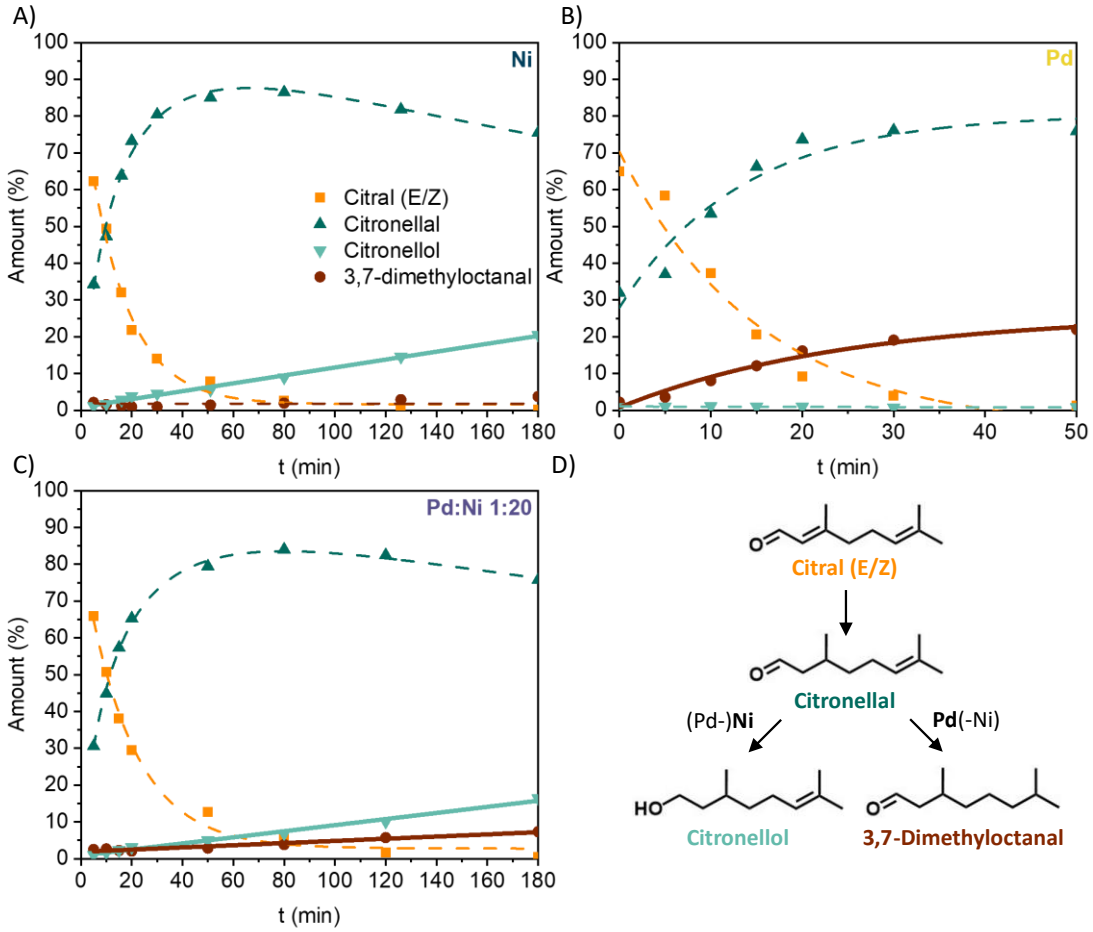

Figure 15. Relative amounts of citral, citronellal, citronellol, and 3,7-dimethyloctanal during the selective hydrogenation of citral, catalyzed by A) Ni/SBA-15, B) Pd/SBA-15, and C) Pd-Ni/SBA-15 Pd:Ni 1:20. D) General reaction scheme based on the reaction profiles in A-C. Conditions: 60 ˚C, 30 bar H_2 (g), 800 rpm stirring rate, 96 mM citral in 2-propanol, 10-35 mg catalyst (0.5 mg Pd).

that in this reaction the leached metal species of the Pd-Ni/SBA-15 catalysts are still bimetallic in nature. Figure 17 shows this for the Pd:Ni 1:10 sample. It suggests a different leaching mechanism. A variety of factors could be the cause, including the reaction temperature (60 ˚C compared to 80 ˚C in CAL hydrogenation) and the interaction of the catalyst surface with the reactant and/or products.

The ICP-OES data on fresh and used Ni/SBA-15, Pd/SBA-15, and Pd-Ni/SBA-15 (Pd:Ni 1:20, 1:15, 1:10, and 1:7) catalysts are presented in Table 6. Compared to the monometallic Pd sample, all bimetallic catalysts lose relatively less Pd during the reaction. These results confirm that the Pd-Ni/SBA-15 NPs are more resistant to leaching than Pd/SBA-15 in citral hydrogenation. In addition, an increase in Pd leaching is observed with an increasing Pd content in the bimetallic NPs. In literature, Pd leaching is sometimes attributed to solvolysis by a protic polar solvent.[60,84] A possible explanation may, therefore, be that the Pd atoms on the catalyst's surface react with the solvent (2-propanol) and form soluble species. In the bimetallic samples, the Pd atoms are coordinated with Ni. This can stabilize them. The same theory might apply to the catalysts in the hydrogenation of CAL, as this reaction was also performed in 2-propanol.

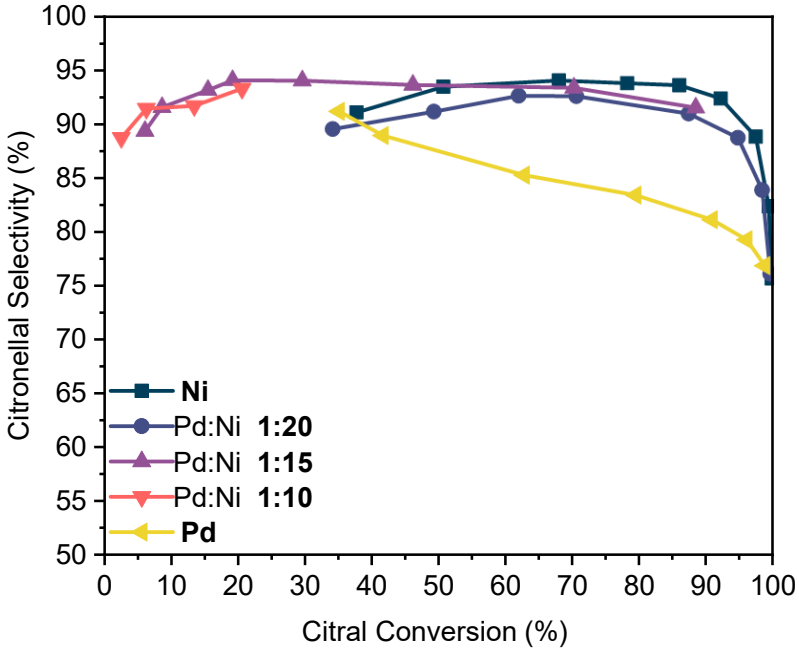

Figure 16. Citronellal selectivity as a function of the citral conversion in the hydrogenation of citral for Pd/SBA-15, Ni/SBA-15, and Pd-Ni/SBA-15 catalysts with different Pd:Ni atomic ratios. Conditions: 60 ˚C, 30 bar H_2 (g), 800 rpm stirring rate, 96 mM citral in 2-propanol, 10-35 mg catalyst (0.5 mg Pd).

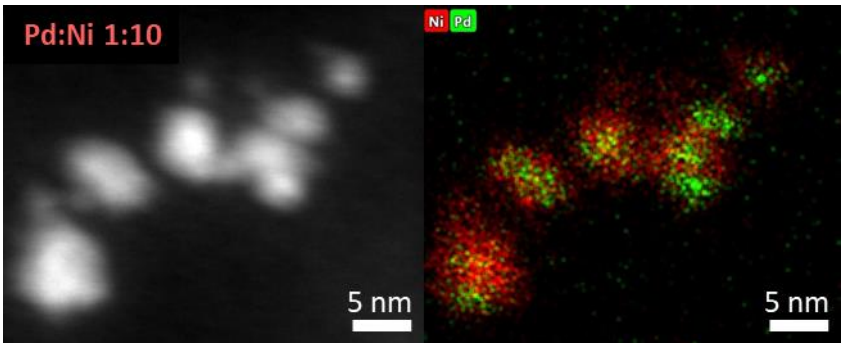

Figure 17. HAADF STEM image (left) and EDX map (right) of a used Pd-Ni/SBA-15 Pd:Ni 1:10 catalyst after the hydrogenation of citral.

Table 6. Comparison of the Pd:Ni ratios and Pd and Ni weight loadings of fresh and used Ni/SBA-15, Pd/SBA-15, and Pd-Ni/SBA-15 catalysts tested for the hydrogenation of citral.

Fresh **Ratio (Pd:Ni)**	Used **Ratio (Pd:Ni)**	Fresh vs Used **% decrease Pd**	Fresh vs Used **% decrease Ni**
Ni	**Ni**	x	-10.6
1:18.3	**1:18.9**	-3.3	-0.3
1:15.0	**1:15.0**	-8.2	-8.3
1:9.1	**1:10.5**	-21.0	-8.7
Pd	**Pd**	-37.7	x

4.4 2-Methyl-3-butyn-2-ol hydrogenation

The previous sections showed that the catalytic activity was more structure sensitive in the hydrogenation of citral compared to CAL. However, no enhanced activity or selectivity was observed. All catalysts were therefore also tested for a different class of reactions; the selective hydrogenation of 2-methyl-3-butyn-2-ol (MBY).

The TOFs ($M \cdot s^{-1} \cdot$ mol surface $metal^{-1}$) of the Pd/SBA-15, Ni/SBA-15, and Pd-Ni/SBA-15 catalysts are plotted against the Pd content in Figure 18. The dashed line represents an additive relationship between the Pd content of the NPs and the activity. Note the logarithmic scale on the vertical axis. The same procedure as for the previously discussed reactions was used to calculate the TOFs, only here a 0^{th} order dependency on the reactant concentration was assumed based on the reaction profiles. Similar to in the hydrogenation of citral, the activity of the bimetallic catalysts drops with an increasing Pd content. However, compared to Ni/SBA-15, the TOFs of the Pd-Ni/SBA-15 Pd:Ni 1:20 and 1:15 catalysts are higher. The Pd:Ni 1:20 NPs have a turnover frequency close to the dashed in the figure, indicating that adding minor amounts of Pd to Ni/SBA-15 could be an effective way to increase the activity in the hydrogenation of MBY.

The adverse effect of the Pd content on the activity of the bimetallic catalysts may be explained analogous to in the hydrogenation of citral. Only in this reaction, strongly adsorbed C≡C and/or C=C bonds would be responsible for active site blockages. Oligomers on the catalyst surface may also play a role, as oligomerization is linked to strongly absorbed C≡C/C=C groups.[50,55]

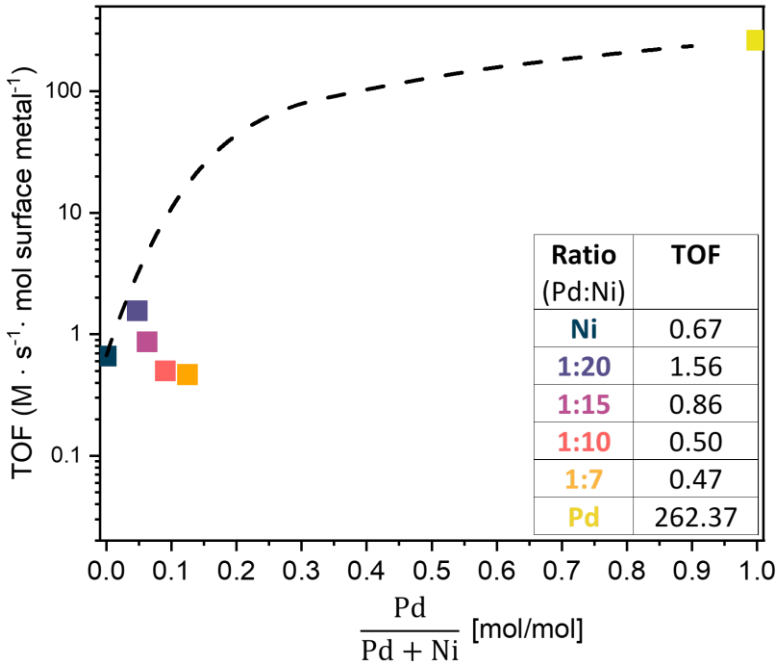

Figure 18. Apparent turnover frequencies (TOFs) of Pd/SBA-15, Ni/SBA-15, and Pd-Ni/SBA-15 catalysts with different Pd:Ni atomic ratios in the selective hydrogenation of 2-methyl-3-butyn-2-ol (MBY). The TOFs are plotted against the Pd content of the NPs. The dashed line is a guide to the eye that represents an additive relationship between the Pd content and the activity (note the logarithmic scale on the vertical axis). Conditions: 50 ˚C, 30 bar H_2 (g), 800 rpm stirring rate, 250 mM MBY in toluene, 10-35 mg catalyst (0.5 mg Pd).

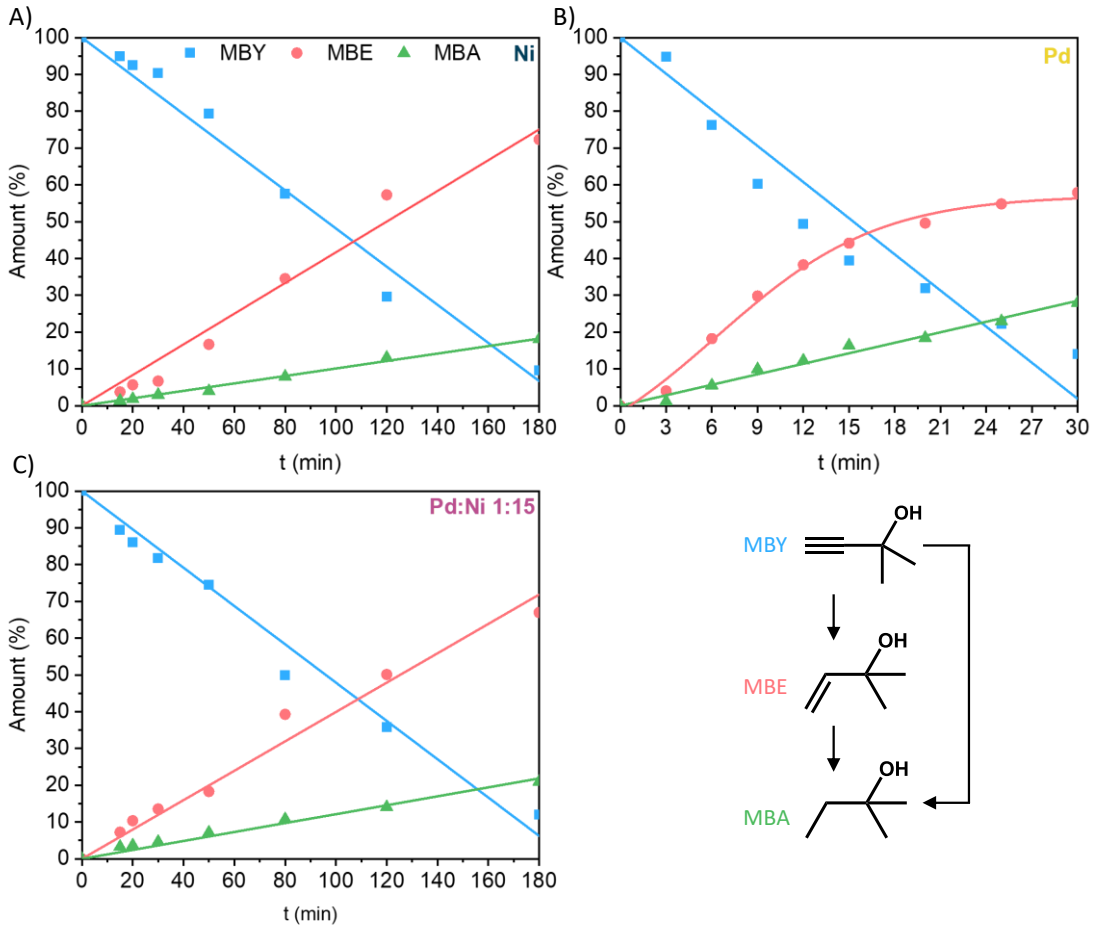

Figure 19. Relative amounts of 2-methyl-3-butyn-2-ol (MBY), 2-methyl-3-buten-2-ol (MBE), and 2-methyl-3-butan-2-ol (MBA) during the selective hydrogenation of MBY, catalyzed by A) Ni/SBA-15, B) Pd/SBA-15, and C) Pd-Ni/SBA-15 Pd:Ni 1:15. Conditions: 50 ˚C, 30 bar H_2 (g), 800 rpm stirring rate, 250 mM MBY in toluene, 10-35 mg catalyst (0.5 mg Pd).

The composition of the reaction mixture over time is shown in Figure 19 for the Pd/SBA-15, Ni/SBA-15, and Pd-Ni/SBA-15 Pd:Ni 1:15 catalyst. This bimetallic sample is representative for all Pd:Ni ratios (Appendix E). All catalysts show similar behavior. However, the MBE concentration stops increasing linearly when approximately 45% MBY is left for the Pd/SBA-15 catalyst. This suggests that at low MBY concentrations, the Pd NPs favor MBA formation more.

The poor C≡C bond selectivity of Pd/SBA-15 at low MBY concentrations is confirmed in Figure 20, which displays the selectivity to MBE against the MBY conversion for each catalyst. This low selectivity is probably influenced by the Pd particle size (1.5 ± 0.5 nm), as undercoordinated sites in small Pd NPs (< 3 nm) promote MBA formation.[85] All bimetallic catalysts are generally more selective, especially at high levels of MBY conversion. No trend between the Pd content and the selectivity is observed. Notably, the Pd-Ni/SBA-15 Pd:Ni 1:20 and 1:15 NPs seem more selective to MBE than there monometallic counterparts (see dashed line in the figure). The difference between their selectivity and that of Ni/SBA-15 is, however, small (1-3 %). Therefore, instead of synergistic effects, experimental errors could be the cause.

TEM analysis of all used catalysts showed no evidence of leaching. The absence of a protic polar solvent may have prevented this deactivation mechanism. The ICP-OES results were inconclusive and can be found in Appendix F.

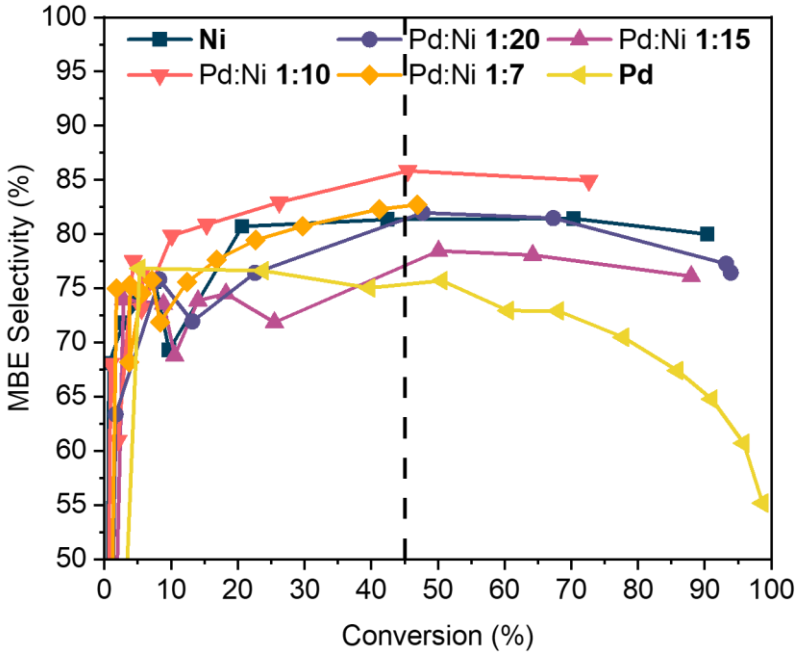

Figure 20. 2-Methyl-3-buten-2-ol (MBE) selectivity as a function of the 2-methyl-3-butyn-2-ol (MBY) conversion in the hydrogenation of MBY for Pd/SBA-15, Ni/SBA-15, and Pd-Ni/SBA-15 NPs of different Pd:Ni atomic ratios. Conditions: 50 ˚C, 30 bar H_2 (g), 800 rpm stirring rate, 150 mM MBY in toluene, 10-35 mg catalyst (0.5 mg Pd).

5

Conclusions

In this thesis, we prepared Pd-Ni/SBA-15 model catalysts of different Pd:Ni ratios and studied the effects of composition on catalytic activity, selectivity, and stability in selective hydrogenation reactions. Alloyed NPs with Pd:Ni atomic ratios of 1:20, 1:15, 1:10, and 1:7 were prepared by incipient wetness (co-)impregnation of SBA-15, as well as monometallic reference catalysts. Characterization with HAADF STEM(-EDX), H_2-TPR, and powder XRD revealed that the composition of the Pd-Ni/SBA-15 NPs was successfully modified to the target ratios, without significantly changing the particle size (d = 3.6-3.8 ± 0.8 nm) or nanoscale intimacy of the metals. All NPs were homogeneously distributed over the support. These properties allowed us to study the effects of composition in the liquid phase selective hydrogenation of cinnamaldehyde (CAL), citral, and 2-methyl-3-butyn-2-ol (MBY).

In the hydrogenation of CAL, the activity of the Pd-Ni/SBA-15 NPs additively increased with the Pd concentration. The incorporation of Pd in Ni/SBA-15 led to a slight reduction (1-3 %) in the selectivity to the main product (hydrocinnamaldehyde). All bimetallic catalysts were more resistant to leaching compared to Pd/SBA-15.

In the hydrogenation of citral, the Pd-Ni/SBA-15 catalysts were also more stable. Moreover, the relative amount of leached Pd increased with an increasing Pd content. A similar dependency of the selectivity to the main product (citronellal) on composition was found in this reaction. The distribution of the side products was distinct for the different catalysts; Pd/SBA-15 mainly converted citronellal to 3,7-dimethyloctanal, Ni/SBA-15 further hydrogenated citronellal to citronellol and the bimetallic catalysts did both. Curiously, the Pd-Ni/SBA-15 NPs were all less active than Pd/SBA-15 and Ni/SBA-15. Their activity dropped with an increasing Pd concentration. To investigate the cause, a catalysts with Pd and Ni in separate phases (Pd+Ni/SBA-15 Pd:Ni 1:10) was also tested for the reduction of citral. This sample was considerably more active than its alloyed counterpart, suggesting that the alloying of Pd and Ni and the resulting changes in the electronic and/or geometric properties were responsible for the decreased activity.

In the hydrogenation of MBY, the activity of the Pd-Ni/SBA-15 NPs also dropped with an increasing Pd content. However, the Pd:Ni 1:20 and 1:15 catalysts were more active than

Ni/SBA-15. In general, the selectivity of the bimetallic catalysts was higher and more stable than that of Pd/SBA-15. No evidence of leaching was found for this reaction.

Our work demonstrates the importance of selecting the right Pd:Ni ratio and model reaction for optimal catalytic performance. These findings could translate to other bimetallic systems for selective hydrogenation reactions.

6

Outlook

In the hydrogenation of citral and 2-methyl-3-butyn-2-ol (MBY), active site blocking by strongly adsorbed function groups was speculated to cause the decreasing activity of Pd-Ni/SBA-15 NPs with an increasing Pd content. In future work, this theory may be verified by employing InfraRed (IR) spectroscopy to measure the bond vibrations of adsorbed species. Additionally, Density Functional Theory (DFT) calculations on the binding strengths of the functional groups on the surface of the different catalysts could help to gain insights into which function group(s) is/are responsible for active site blocking. For the same purpose, the Pd-Ni/SBA-15 catalysts can be tested for the hydrogenation of compounds similar to citral and MBY, but with less/different functional groups (e.g. 3,7-dimethyloctanal or 2-methyl-3-buten-2-ol).

Contrary to our study, other reports on Pd-Ni NP structure-performance relationships in the hydrogenation of α,β-unsaturated aldehydes described synergistic activities and selectivities. The NPs in these works contained relatively more Pd compared to the bimetallic catalysts used here. It would, therefore, be interesting to prepare Pd-Ni/SBA-15 catalysts with a lower Pd:Ni ratio and test them for the hydrogenation of cinnamaldehyde (CAL) and citral.

One of the most promising properties of the Pd-Ni/SBA-15 catalysts was their greater resistance to leaching compared to Pd/SBA-15. This may be further investigated with hot filtration and recycling tests. With the former method, the activity-contribution of the leached species can be determined. The latter may show that the catalytic performance of the bimetallic catalysts is less affected by leaching compared to Pd/SBA-15 in consecutive tests. It might also reveal differences between the Pd-Ni/SBA-15 samples.

Finally, although not described in this thesis, we also prepared Pd-Ni/SBA-15 Pd:Ni 1:10 NPs with three distinct particle sizes within the critical size range of 1-5 nm. This was achieved by a combination of increasing the pore size of the support and the metal loading. These samples could be used to study particle size effects in the different reactions.

Acknowledgements

This thesis would not have been possible without the help of many people. First, I would like to thank my daily supervisor Kristiaan Helfferich. It was a great pleasure to be part of the Pd-Ni team this past year. You always made me feel like you had all the time in the world to help and teach me – no matter how busy you were. I learned an unimaginable amount of things from you and truly enjoyed all of our discussions related (and unrelated) to this project. Second, I would like to thank Petra de Jongh and Jessi van der Hoeven for their role as my examiners and for all the helpful feedback and suggestions. Many thanks to Remco Dalebout, Dennie Wezendonk, and Jan Willem de Rijk for the technical support and trainings. You were truly indispensable. I would also like to thank Hans Meeldijk for making the EM images in this thesis possible. Alex van Silfhout, thank you for the VSM measurements. I learned a lot from you. Juliette Verschoor is gratefully acknowledged for teaching me how to use the XRD dome. Finally, I want to express my sincere appreciation for all people at MCC for contributing to a pleasant work environment.

Bibliography

1. Irfan, Muhammad, Toma N. Glasnov, and C. Oliver Kappe. "Heterogeneous catalytic hydrogenation reactions in continuous-flow reactors." *ChemSusChem* 4.3 (2011): 300-316.

2. Strekalova, Anna A., Anastasiya A. Shesterkina, and Leonid M. Kustov. "Recent progress in hydrogenation of esters on heterogeneous bimetallic catalysts." *Catalysis Science & Technology* 11.22 (2021): 7229-7238.

3. Meemken, Fabian, and Alfons Baiker. "Recent Progress in Heterogeneous Asymmetric Hydrogenation of C=O and C=C Bonds on Supported Noble Metal Catalysts." *Chemical reviews* 117.17 (2017): 11522-11569.

4. Lan, Xiaocheng, and Tiefeng Wang. "Highly selective catalysts for the hydrogenation of unsaturated aldehydes: a review." *ACS Catalysis* 10.4 (2020): 2764-2790.

5. Lucarelli, Carlo, and Angelo Vaccari. "Examples of heterogeneous catalytic processes for fine chemistry." *Green chemistry* 13.8 (2011): 1941-1949.

6. Sápi, András, et al. "Metallic nanoparticles in heterogeneous catalysis." *Catalysis Letters* 151 (2021): 2153-2175.

7. Stoffels, Marius A., et al. "Technology trends of catalysts in hydrogenation reactions: a patent landscape analysis." *Advanced synthesis & catalysis* 362.6 (2020): 1258-1274.

8. Ndolomingo, Matumuene Joe, Ndzondelelo Bingwa, and Reinout Meijboom. "Review of supported metal nanoparticles: synthesis methodologies, advantages and application as catalysts." *Journal of Materials Science* 55.15 (2020): 6195-6241.

9. Gómez-López, Paulette, et al. "Nanomaterials and catalysis for green chemistry." *Current Opinion in Green and Sustainable Chemistry* 24 (2020): 48-55.

10. Zhang, Leilei, et al. "Selective hydrogenation over supported metal catalysts: from nanoparticles to single atoms." *Chemical reviews* 120.2 (2019): 683-733.

11. Notar Francesco, Irene, Fabien Fontaine-Vive, and Sylvain Antoniotti. "Synergy in the catalytic activity of bimetallic nanoparticles and new synthetic methods for the preparation of fine chemicals." *ChemCatChem* 6.10 (2014): 2784-2791.

12. Chen, Bingfeng, et al. "Tuning catalytic selectivity of liquid-phase hydrogenation of furfural via synergistic effects of supported bimetallic catalysts." *Applied Catalysis A: General* 500 (2015): 23-29.

13. Zhu, Jiadong, et al. "Ni–In synergy in CO_2 hydrogenation to methanol." *ACS catalysis* 11.18 (2021): 11371-11384.

14 Singh, Ashish Kumar, and Qiang Xu. "Synergistic catalysis over bimetallic alloy nanoparticles." *ChemCatChem* 5.3 (2013): 652-676.

15. Coq, Bernard, and François Figueras. "Bimetallic palladium catalysts: influence of the co-metal on the catalyst performance." *Journal of Molecular Catalysis A: Chemical* 173.1-2 (2001): 117-134.

16. Liu, Lichen, and Avelino Corma. "Metal catalysts for heterogeneous catalysis: from single atoms to nanoclusters and nanoparticles." *Chemical reviews* 118.10 (2018): 4981-5079.

17. Furukawa, Shinya, and Takayuki Komatsu. "Selective hydrogenation of functionalized alkynes to (E)-alkenes, using ordered alloys as catalysts." *ACS Catalysis* 6.3 (2016): 2121-2125.

18. Guczi, László. "Bimetallic nano-particles: featuring structure and reactivity." *Catalysis Today* 101.2 (2005): 53-64.

19. Tao, Franklin Feng. "Synthesis, catalysis, surface chemistry and structure of bimetallic nanocatalysts." *Chemical Society Reviews* 41.24 (2012): 7977-7979.

20. Wu, Jianbo, et al. "Surface lattice-engineered bimetallic nanoparticles and their catalytic properties." *Chemical Society Reviews* 41.24 (2012): 8066-8074.

21. van der Hoeven, Jessi ES, et al. "Unlocking synergy in bimetallic catalysts by core–shell design." *Nature Materials* 20.9 (2021): 1216-1220.

22. Zhao, Xiaojing, et al. "Recent Progress in Pd-Based Nanocatalysts for Selective Hydrogenation." *Acs Omega* 7.1 (2021): 17-31.

23. Goulas, Konstantinos A., et al. "Selectivity tuning over monometallic and bimetallic dehydrogenation catalysts: effects of support and particle size." *Catalysis Science & Technology* 8.1 (2018): 314-327.

24. Mao, Shanjun, et al. "Geometric and Electronic Effects in Hydrogenation Reactions." *ACS Catalysis* 13 (2022): 974-1019.

25. Fan, Jiaxuan, et al. "Recent progress on rational design of bimetallic Pd based catalysts and their advanced catalysis." *ACS Catalysis* 10.22 (2020): 13560-13583.

26. Yamanaka, Nobutaka, and Shogo Shimazu. "Selective hydrogenation properties of Ni-based bimetallic catalysts." *Eng* 3.1 (2022): 60-77.

27. Hou, Ruijun, et al. "Selective hydrogenation of 1, 3-butadiene on PdNi bimetallic catalyst: From model surfaces to supported catalysts." *Journal of catalysis* 316 (2014): 1-10.

28. Liu, Chunling, et al. "Facile synthesis and synergistically acting catalytic performance of supported bimetallic PdNi nanoparticle catalysts for selective hydrogenation of citral." *Molecular Catalysis* 436 (2017): 237-247.

29. Wang, Dingsheng, and Yadong Li. "Bimetallic nanocrystals: liquid-phase synthesis and catalytic applications." *Advanced Materials* 23.9 (2011): 1044-1060.

30. Sankar, Meenakshisundaram, et al. "Designing bimetallic catalysts for a green and sustainable future." *Chemical Society Reviews* 41.24 (2012): 8099-8139.

31. Mehrabadi, Bahareh AT, et al. "A review of preparation methods for supported metal catalysts." *Advances in catalysis* 61 (2017): 1-35.

32. Gu, Jun, Ya-Wen Zhang, and Franklin Feng Tao. "Shape control of bimetallic nanocatalysts through well-designed colloidal chemistry approaches." *Chemical Society Reviews* 41.24 (2012): 8050-8065.

33. Loza, Kateryna, Marc Heggen, and Matthias Epple. "Synthesis, structure, properties, and applications of bimetallic nanoparticles of noble metals." *Advanced functional materials* 30.21 (2020): 1909260.

34. Munnik, Peter, Petra E. De Jongh, and Krijn P. De Jong. "Recent developments in the synthesis of supported catalysts." *Chemical reviews* 115.14 (2015): 6687-6718.

35. Han, Shiying, et al. "Improvement effect of Ni to Pd-Ni/SBA-15 catalyst for selective hydrogenation of cinnamaldehyde to hydrocinnamaldehyde." *Catalysts* 8.5 (2018): 200.

36. González-Fernández, Alberto, Chiara Pischetola, and Fernando Cardenas-Lizana. "Gas-phase catalytic hydrogenation/isomerization in the transformation of 3-butyn-2-ol over Pd-Ni/Al2O3." *The Journal of Physical Chemistry C* 125.4 (2021): 2454-2463.

37. Li, Yanping, et al. "Bimetallic NiPd/SBA-15 alloy as an effective catalyst for selective hydrogenation of CO2 to methane." *International Journal of Hydrogen Energy* 44.26 (2019): 13354-13363.

38. Van Dillen, A. Jos, et al. "Synthesis of supported catalysts by impregnation and drying using aqueous chelated metal complexes." *Journal of Catalysis* 216.1-2 (2003): 257-264.

39. Wei, Zhehao, et al. "Bimetallic catalysts for hydrogen generation." *Chemical Society Reviews* 41.24 (2012): 7994-8008.

40. Edwards, Jennifer K., et al. "The effect of heat treatment on the performance and structure of carbon-supported Au–Pd catalysts for the direct synthesis of hydrogen peroxide." *Journal of catalysis* 292 (2012): 227-238.

41. Qin, Qiang, and Doraiswam Ramkrishna. "The effect of operating conditions on the dispersion state of supported metal catalysts: A model study." *Industrial & engineering chemistry research* 44.16 (2005): 6466-6476.

42. Luneau, Mathilde, et al. "Guidelines to achieving high selectivity for the hydrogenation of α, β-unsaturated aldehydes with bimetallic and dilute alloy catalysts: a review." *Chemical reviews* 120.23 (2020): 12834-12872.

43. Gallezot, P., and D. Richard. "Selective hydrogenation of α, β-unsaturated aldehydes." *Catalysis Reviews* 40.1-2 (1998): 81-126.

44. Yuan, Yuan, et al. "Recent progress in chemoselective hydrogenation of α, β-unsaturated aldehyde to unsaturated alcohol over nanomaterials." *Current Organic Chemistry* 17.4 (2013): 400-413.

45. Fuggle, John C., et al. "Electronic structure of Ni and Pd alloys. I. X-ray photoelectron spectroscopy of the valence bands." *Physical Review B* 27.4 (1983): 2145.

46. Wang, Xiaofeng, et al. "Recent advances in selective hydrogenation of cinnamaldehyde over supported metal-based catalysts." *ACS Catalysis* 10.4 (2020): 2395-2412.

47. Jiang, Feng, et al. "Particle size effects in the selective hydrogenation of cinnamaldehyde over supported palladium catalysts." *RSC advances* 6.79 (2016): 75541-75551.

48. Stolle, Achim, et al. "Hydrogenation of citral: a wide-spread model reaction for selective reduction of α, β-unsaturated aldehydes." *RSC advances* 3.7 (2013): 2112-2153.

49. Syunbayev, U., et al. "The liquid-phase hydrogenation of citral to citronellal at hydrogen pressure." *International Journal of Chemical Engineering and Applications* 7.2 (2016): 133.

50. Chen, Xiao, Chuang Shi, and Changhai Liang. "Highly selective catalysts for the hydrogenation of alkynols: A review." *Chinese Journal of Catalysis* 42.12 (2021): 2105-2121.

51. Wang, Zhe, et al. "Fundamental aspects of alkyne semi-hydrogenation over heterogeneous catalysts." *Nano Research* 15.12 (2022): 10044-10062.

52. Cherkasov, Nikolay, et al. "Palladium–bismuth intermetallic and surface-poisoned catalysts for the semi-hydrogenation of 2-methyl-3-butyn-2-ol." *Applied Catalysis A: General* 497 (2015): 22-30.

53. Semagina, N., Renken, A., Laub, D. & Kiwi-Minsker, L. Synthesis of monodispersed palladium nanoparticles to study structure sensitivity of solvent-free selective hydrogenation of 2-methyl-3-butyn-2-ol. *J Catal* **246**, 308–314 (2007).

54. Semagina, Natalia, et al. "Structured catalyst of Pd/ZnO on sintered metal fibers for 2-methyl-3-butyn-2-ol selective hydrogenation." *Journal of Catalysis* 251.1 (2007): 213-222.

55. Crespo-Quesada, M., Cárdenas-Lizana, F., Dessimoz, A. L. & Kiwi-Minsker, L. Modern trends in catalyst and process design for alkyne hydrogenations. *ACS Catal* **2**, 1773–1786 (2012).

56. Prestianni, A. *et al.* Structure sensitivity of 2-methyl-3-butyn-2-ol hydrogenation on Pd: Computational and experimental modeling. *Journal of Physical Chemistry C* **118**, 3119–3128 (2014).

57. Martín, Antonio J., et al. "Unifying views on catalyst deactivation." *Nature Catalysis* 5.10 (2022): 854-866.

58. Besson, Michele, and Pierre Gallezot. "Deactivation of metal catalysts in liquid phase organic reactions." *Catalysis Today* 81.4 (2003): 547-559.

59. Arai, M. & Zhao, F. Metal Catalysts Recycling and Heterogeneous/Homogeneous Catalysis. *Catalysts 2015, Vol. 5, Pages 868-870* **5**, 868–870 (2015).

60. Sádaba, Irantzu, et al. "Deactivation of solid catalysts in liquid media: the case of leaching of active sites in biomass conversion reactions." *Green Chemistry* 17.8 (2015): 4133-4145.

61. Hii, King Kuok, and Klaus Hellgardt. "Catalysis in flow: why leaching matters." *Organometallic Flow Chemistry* (2016): 249-262.

62. Sievers, Carsten, et al. "Phenomena affecting catalytic reactions at solid–liquid interfaces." *ACS Catalysis* 6.12 (2016): 8286-8307.

63. Arends, I. W. C. E., and R. A. Sheldon. "Activities and stabilities of heterogeneous catalysts in selective liquid phase oxidations: recent developments." *Applied Catalysis A: General* 212.1-2 (2001): 175-187.

64. Phan, Nam TS, Matthew Van Der Sluys, and Christopher W. Jones. "On the nature of the active species in palladium catalyzed Mizoroki–Heck and Suzuki–Miyaura couplings–homogeneous or heterogeneous catalysis, a critical review." *Advanced Synthesis & Catalysis* 348.6 (2006): 609-679.

65. Panpranot, Joongjai, et al. "A comparative study of Pd/SiO2 and Pd/MCM-41 catalysts in liquid-phase hydrogenation." *Catalysis Communications* 5.10 (2004): 583-590.

66. Lamblin, Marc, et al. "Recyclable heterogeneous palladium catalysts in pure water: Sustainable developments in Suzuki, Heck, Sonogashira and Tsuji–Trost reactions." *Advanced Synthesis & Catalysis* 352.1 (2010): 33-79.

67. Van Vaerenbergh, Beau, et al. "Towards high-performance heterogeneous palladium nanoparticle catalysts for sustainable liquid-phase reactions." *Reaction Chemistry & Engineering* 5.9 (2020): 1556-1618.

68. Mironenko, Roman M., et al. "Comparing Separation vs. Fresh Start to Assess Reusability of Pd/C Catalyst in Liquid-Phase Hydrogenation." *ChemCatChem* 13.16 (2021): 3656-3661.

69. Heshmatpour, Felora, and Reza Abazari. "Formation of dispersed palladium–nickel bimetallic nanoparticles in microemulsions: synthesis, characterization, and their use as efficient heterogeneous recyclable catalysts for the amination reactions of aryl chlorides under mild conditions." RSC Advances 4.99 (2014): 55815-55826.

70. Niakan, Mahsa, and Majid Masteri-Farahani. "Pd–Ni bimetallic catalyst supported on dendrimer-functionalized magnetic graphene oxide for efficient catalytic Suzuki-Miyaura coupling reaction." *Tetrahedron* 108 (2022): 132655.

71. Xia, Haian, et al. "Efficient hydrogenation of xylose and hemicellulosic hydrolysate to xylitol over Ni-Re bimetallic nanoparticle catalyst." *Nanomaterials* 10.1 (2019): 73.

72. Zhang, Li, et al. "Hydrogenation of levulinic acid into gamma-valerolactone over in situ reduced CuAg bimetallic catalyst: Strategy and mechanism of preventing Cu leaching." *Applied Catalysis B: Environmental* 232 (2018): 1-10.

73. Lee, Hyung Ik, et al. "Morphology-selective synthesis of mesoporous SBA-15 particles over micrometer, submicrometer and nanometer scales." *Journal of Materials Chemistry* 20.39 (2010): 8483-8487.

74. Muniz, Francisco Tiago Leitao, et al. "The Scherrer equation and the dynamical theory of X-ray diffraction." *Acta Crystallographica Section A: Foundations and Advances* 72.3 (2016): 385-390.

75. Ameh, E. S. "A review of basic crystallography and x-ray diffraction applications." *The international journal of advanced manufacturing technology* 105 (2019): 3289-3302.

76. Mierczynski, Pawel, et al. "High active and selective Ni/CeO2–Al2O3 and Pd–Ni/CeO2–Al2O3 catalysts for oxy-steam reforming of methanol." *Catalysts* 8.9 (2018): 380.

77. Insorn, Paisan, and Boonyarach Kitiyanan. "Selective hydrogenation of mixed C4 containing high vinyl acetylene by Mn-Pd, Ni-Pd and Ag-Pd on Al2O3 catalysts." *Catalysis Today* 256 (2015): 223-230.

78. Feeley, Jennifer Schaefer, and Wolfgang MH Sachtler. "Palladium-enhanced reducibility of nickel in NaY." *Zeolites* 10.8 (1990): 738-745.

79. Zhu, Huaqing, et al. "Pd/CeO2–TiO2 catalyst for CO oxidation at low temperature: a TPR study with H2 and CO as reducing agents." *Journal of Catalysis* 225.2 (2004): 267-277.

80. Chen, H., N. E. Brener, and J. Callaway. "Electronic structure, optical and magnetic properties of fcc palladium." *Physical Review B* 40.3 (1989): 1443.

81. Mäki-Arvela, P., et al. "Chemoselective hydrogenation of carbonyl compounds over heterogeneous catalysts." *Applied Catalysis A: General* 292 (2005): 1-49.

82. Singh, Utpal K., and M. Albert Vannice. "Liquid-phase citral hydrogenation over SiO2-supported group VIII metals." *Journal of Catalysis* 199.1 (2001): 73-84.

83. Burgener, Marco, et al. "Nature of catalyst deactivation during citral hydrogenation: a catalytic and ATR-IR study." *Journal of Catalysis* 228.1 (2004): 152-161.

84. Chang, Chun-Ran, et al. "Theoretical study on the leaching of palladium in a CO atmosphere." *Catalysis Science & Technology* 2.11 (2012): 2238-2248.

85. Crespo-Quesada, Micaela, et al. "Structure sensitivity of alkynol hydrogenation on shape-and size-controlled palladium nanocrystals: which sites are most active and selective?." *Journal of the American Chemical Society* 133.32 (2011): 12787-12794.

Appendices

Appendix A

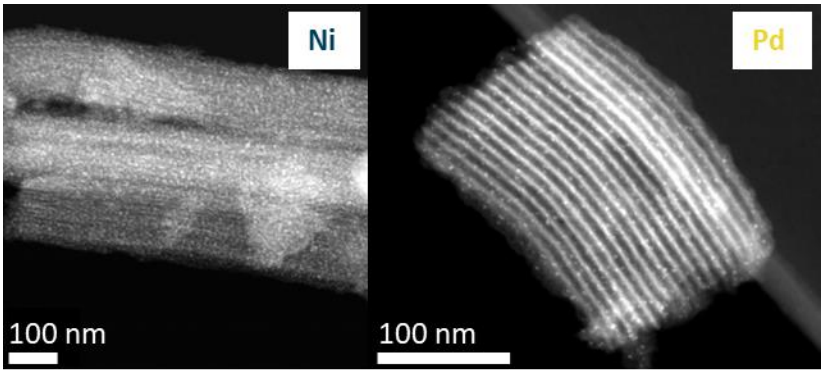

Figure A1. HAADF STEM images of a Ni/SBA-15 (left) and Pd/SBA-15 (right) catalyst. The NPs are homogeneously distributed over the support.

Appendix B

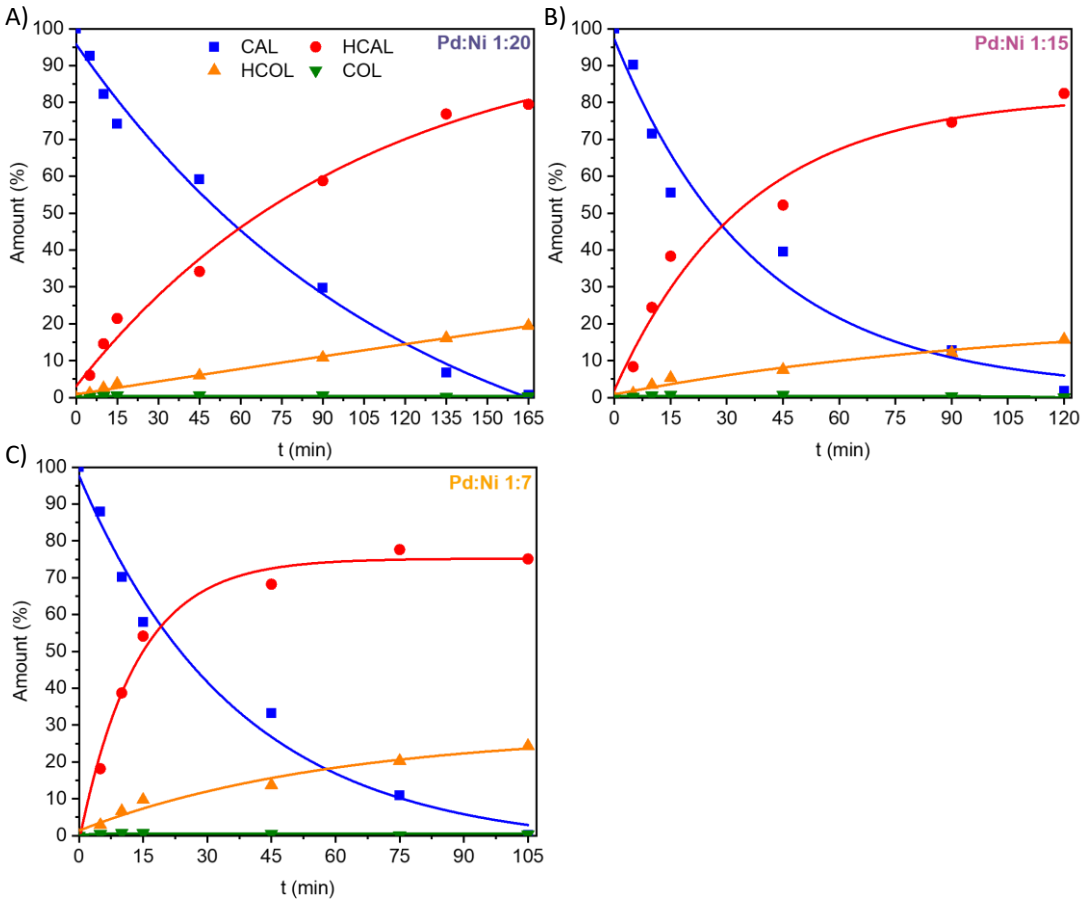

Figure A2. Relative amounts of cinnamaldehyde (CAL), hydrocinnamaldehyde (HCAL), cinnamic alcohol (COL), and hydrocinnamic alcohol (HCOL) during the selective hydrogenation of CAL, catalyzed by a Pd-Ni/SBA-15 Pd:Ni A) 1:20, B) 1:15, and C) 1:7 catalyst. Conditions: 80 ˚C, 30 bar H_2 (g), 800 rpm stirring rate, 147 mM CAL in 2-propanol, 25 mg catalyst.

Appendix C

A bimetallic catalyst with Pd and Ni in separate phases (Pd+Ni/SBA-15 Pd:Ni 1:10) was also tested for the hydrogenation of citral. HAADF STEM imaging with EDX mapping revealed finely dispersed Ni clusters (< 2 nm) with considerably larger (4.3 nm) Pd NPs, as shown in Figure A3.

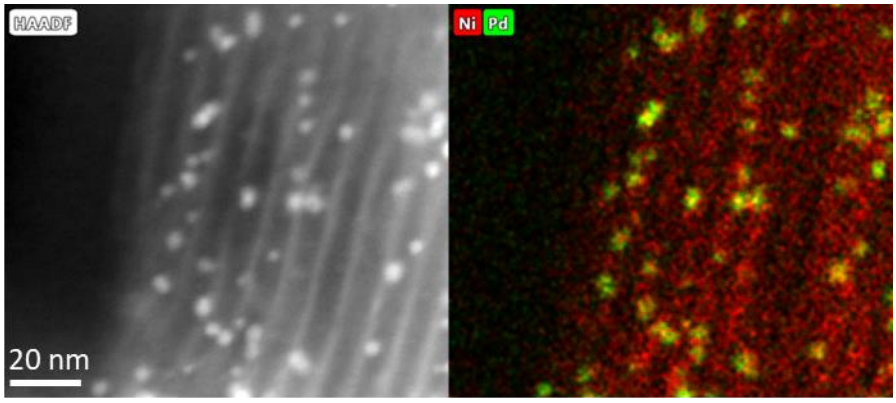

Figure A3. HAADF STEM image (left) and EDX map (right) of the Pd+Ni/SBA-15 Pd:Ni 1:10 catalysts, in which the Pd and Ni are in separate phases.

Table A1 shows the activity, expressed in TOF (s^{-1} · mol surface $metal^{-1}$), of the Ni/SBA-15, Pd/SBA-15, Pd+Ni/SBA-15, and the Pd-Ni/SBA-15 Pd:Ni 1:10 catalysts. The TOF of the Pd+Ni/SBA-15 sample is over 25 times higher than the TOF of the alloyed Pd-Ni NPs. This confirms that the alloying of Pd and Ni plays a role in the loss of activity of Pd-Ni/SBA-15 compared to its monometallic counterparts. The Pd+Ni/SBA-15 catalyst sample is still noticeably less active than Pd/SBA-15 and Ni/SBA-15. However, an estimated 40-70% of this catalyst remained inside the XCAD during the run, thus preventing it from participating in the reaction.

The selectivity to the main product (citronellal) is plotted against the citral conversion in Figure A4. The selectivity of the Pd+Ni/SBA-15 catalyst is consistently lower than that of all the bimetallic alloyed catalysts. This implies that alloying also affects the selectivity.

Table A1. Apparent turnover frequencies (TOFs) of a Ni/SBA-15, Pd/SBA-15, Pd-Ni/SBA-15 Pd:Ni 1:10, and Pd+Ni/SBA-15 Pd:Ni 1:10 catalyst in the selective hydrogenation of citral. Conditions: 60 ˚C, 30 bar H_2 (g), 800 rpm stirring rate, 96 mM citral in 2-propanol, 10-35 mg catalyst (0.5 mg Pd).

Sample (Pd:Ni)	**TOF** (s^{-1}·mol surface $metal^{-1}$)
Ni	50.7
1:10	1.1
Pd+Ni (1:10)	25.8
Pd	185.3

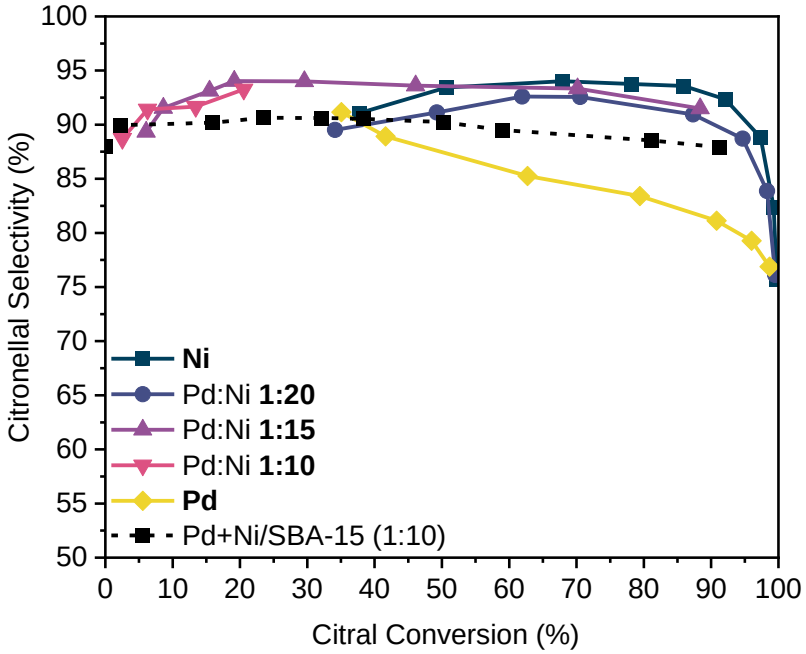

Figure A4. Citronellal selectivity versus the citral conversion in the hydrogenation of citral for Pd/SBA-15, Ni/SBA-15, Pd+Ni/SBA-15, and Pd-Ni/SBA-15 nanocatalysts of different compositions. Conditions: 60 ˚C, 30 bar H_2 (g), 800 rpm stirring rate, 96 mM citral in 2-propanol, 10-35 mg catalyst (0.5 mg Pd).

Appendix D

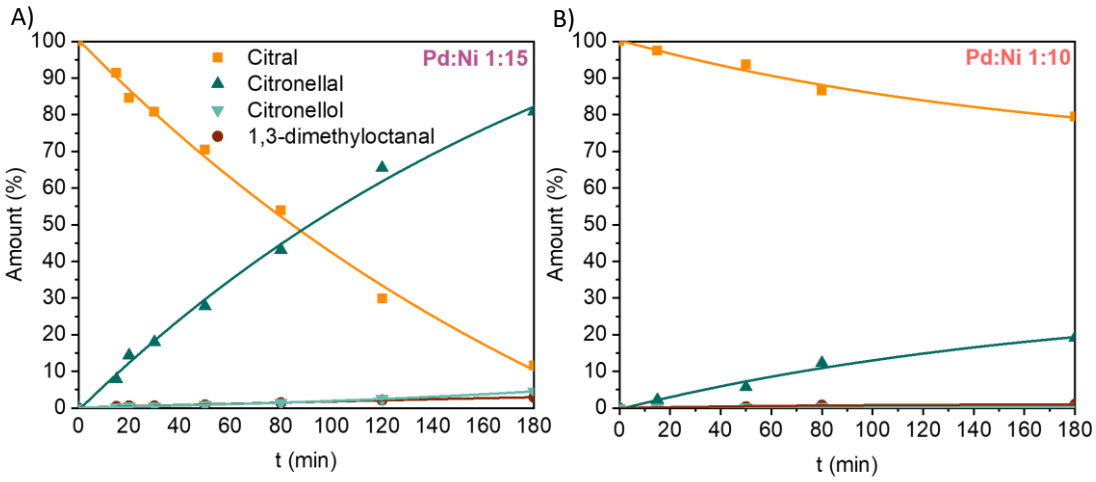

Figure A5. Relative amounts of citral, citronellal, citronellol, and 3,7-dimethyloctanal during the selective hydrogenation of citral, catalyzed by Pd-Ni/SBA-15 Pd:Ni A) 1:15 and B) 1:10. Conditions: 60 ˚C, 30 bar H_2 (g), 800 rpm stirring rate, 96 mM citral in 2-propanol, 23 mg (1:15) and 18 mg (1:10) catalyst (0.5 mg Pd).

Appendix E

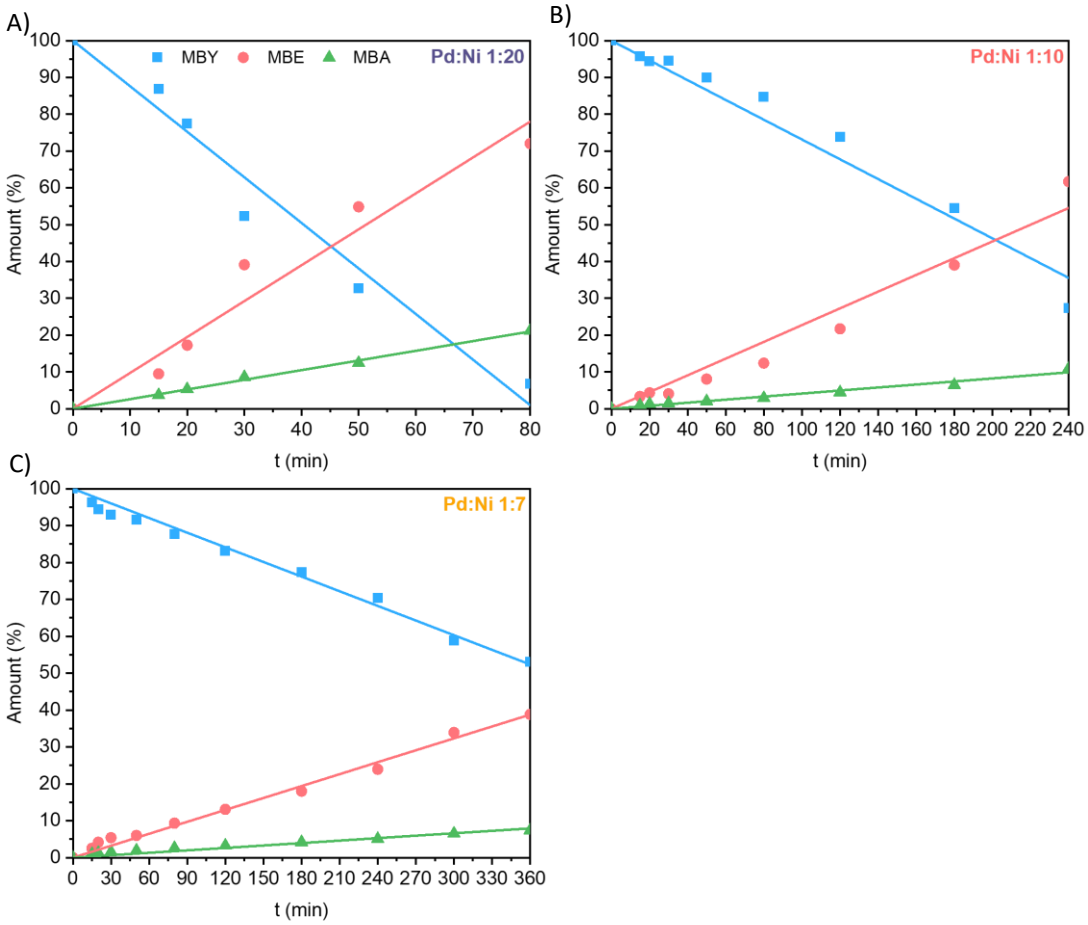

Figure A6. Relative amounts of 2-methyl-3-butyn-2-ol (MBY), 2-methyl-3-buten-2-ol (MBE), and 2-methyl-3-butan-2-ol (MBA) during the selective hydrogenation of MBY, catalyzed by a Pd-Ni/SBA-15 Pd:Ni A) 1:20 B) 1:10, and C) 1:7 catalyst. Conditions: 50 ˚C, 30 bar H_2 (g), 800 rpm stirring rate, 250 mM MBY in toluene, 10-35 mg catalyst (0.5 mg Pd).

Appendix F

The ICP-OES data on fresh and used catalysts after the hydrogenation of 2-methyl-3-butyn-2-ol (MBY) are presented in Table A2. The data suggests that in this reaction, the catalysts are more stable. Curiously, the Pd-Ni/SBA-15 Pd:Ni 1:20 and 1:15 catalysts seem to contain more Pd after the catalytic test than before. These are also the only bimetallic samples of which the turnover frequencies (TOF) are not below that of Ni/SBA-15. However, we do not think that the TOFs of Pd:Ni 1:20 and 1:15 are inaccurate. A new and more elaborate cleaning method was developed to rid of any leached metal species or remaining catalyst. Moreover, blank runs between tests (only reactant, no catalyst) showed no conversion of MBY. We, therefore, think that the unexpected ICP results can be explained by inhomogeneities in the catalyst or the loss of SBA-15.

Table A2. Comparison of the composition and Pd and Ni weight loading of fresh and used Ni/SBA-15, Pd/SBA-15, and Pd-Ni/SBA-15 catalysts with different Pd:Ni ratios tested for the hydrogenation of 2-methyl-3-butyn-2-ol.

Fresh **Ratio (Pd:Ni)**	Used **Ratio (Pd:Ni)**	Fresh vs Used **% decrease Pd**	Fresh vs Used **% decrease Ni**
Ni	**Ni**	x	-8.4
1:18.3	**1:14.3**	+30.1	+2.2
1:15.0	**1:11.5**	+25.9	-3.1
Pd	**Pd**	-9.3	x